Optimal Allocation of Active and Reactive Power Compensators and Voltage Regulators in Modern Distribution Systems

Heba M. Elaraby, Ahmed M. Ibrahim, Muhyaddin Rawa, Essam El-Din Abou El-Zahab, and Shady H. E. Abdel Aleem (iD)

1 Introduction

Renewable energy technology has become the most critical technology in energy feeding systems in most countries to reduce dependence on energy production from traditional fossil fuels. These days, the mature renewable-based technologies are wind turbines, solar, fuel cells, small hydropower, oceans (waves and tides), biomass, and geothermal systems. These technologies have enhanced energy security, affected electricity price fluctuations, reduced gas emissions, and reduced congestion of transmission lines while providing enhanced voltage stability potential to electricity grids. A distributed generator (DG) can be a renewable or non-renewable source and can be networked (grid-connected) or act as a stand-alone

H. M. Elaraby
Electrical Power Department, Faculty of Engineering, Cairo University, Giza, Egypt

Electrical Engineering Department, The Higher Institute for Engineering and Technology, Fifth Settlement, New Cairo, Egypt

A. M. Ibrahim · E. E.-D. A. El-Zahab
Electrical Power Department, Faculty of Engineering, Cairo University, Giza, Egypt

M. Rawa
Center of Research Excellence in Renewable Energy and Power Systems, King Abdulaziz University, Jeddah, Saudi Arabia

Department of Electrical and Computer Engineering, Faculty of Engineering, King Abdulaziz University, Jeddah, Saudi Arabia

S. H. E. Abdel Aleem (✉)
Electrical Engineering and Electronics Department, Valley High Institute of Engineering and Technology, Science Valley Academy, Qalyubia, Egypt
e-mail: engyshady@ieee.org

system. Due to their low investment costs and small sizes, DGs are imperative in modern energy system planning [1].

DGs can be classified as follows [2, 3]: (i) technology basis: they can be categorized into renewable (non-fossil fuel-based) and nonrenewable (fossil fuel-based), (ii) generated power basis: they can be categorized into DGs that generate alternating current (AC) power (wind turbines, microturbines (MTs), and others) and DGs that generate direct current (DC) power (fuel cells (FCs), solar photovoltaics (PV), and others), (iii) supply duration basis: they can be categorized into long duration-based, moderate duration-based, and short duration-based DGs, (iv) capacity basis: they can be categorized into micro decentralized DGs (1 W – 5 kW), small decentralized/centralized DGs (5 kW – 5 MW), medium DGs (5–50 MW) and are almost centralized, and large DGs (50–300 MW) and are centralized, (v) grid interface basis: they can be categorized into inverter-based DGs include PV systems, wind turbine generators (Type 3–Type 5), FCs cells, and MTs, and non-inverter-based DGs which include mini-hydro synchronous and induction generators (Type 1 and Type 2 wind turbines), (vi) power flow model basis: the DGs' output power can be either set to constant power factor (PF) for small decentralized DGs, and the bus at which the DG is connected is modeled as a PQ bus in power flow studies, or to be set to constant voltage for large centralized DGs, and the bus at which the DG is connected is modeled as a PV bus in power flow studies, and (vii) power delivering capability basis in which DGs can only deliver active power at unity PF (e.g., PV, MTs, and FCs). However, according to the current grid codes, PV systems have to provide reactive power, or deliver only reactive power at zero PF (e.g., synchronous compensators), or to deliver active power but consume reactive power (the reactive power Q is –ve), and the PF value is between [0,1]. Induction generators are used in Type 1 and Type 2 wind turbines. Doubly-fed induction generators are used in Type 3 wind turbines and synchronous generators are used in Types 4 and 5. DG classifications are explored in Fig. 1 [1, 4].
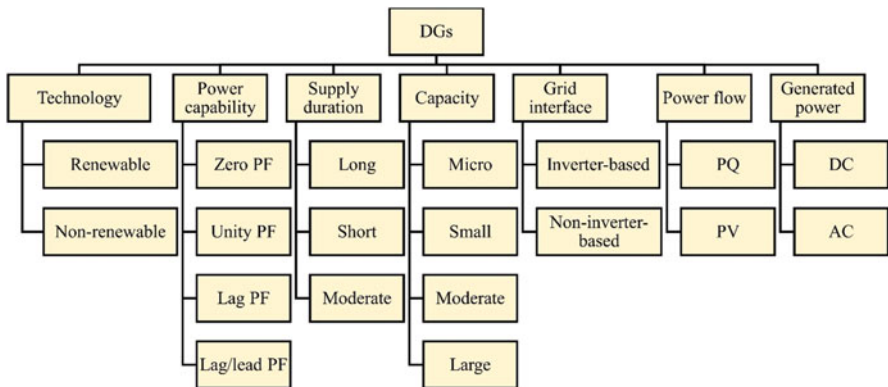

Fig. 1 Classification of DGs

The integration of DGs into RDSs significantly affects the flow of energy and voltage conditions at customers and utility equipment. These effects may be either positive or negative, depending on the distribution systems case and the operating characteristics of DGs [5, 6]. Generally, the positive effects on RDSs have been termed – the supporting benefits – and are bordered as follows [7–9]: active and reactive power loss reduction, reliability enhancement, quality of power (QoP) improvement, voltage stability (VS) enhancement, steady-state voltage profile support, capacity release (transmission and distribution capacities alike), postponements of new or reinforced transmission and distribution infrastructure, easy fitting and connection, and cost reduction. In some cases, integrating DGs at nonoptimal locations with nonoptimal sizes can result in high power losses, system instability, and a boom in operational costs due to poor efficiency and high losses. In addition, the increased renewables penetration increases energy security by expanding (mixing) energy resources, advances self-sufficiency, and boosts flexibility for system operators. Some studies have shown that the presence of DGs that use power electronic-based converters may cause major QoP, overvoltage, overloading, and protection problems, as shown in Fig. 2 that present the recent investigated renewables hosting capacity (HC) problems [6], or simply, the problems that may occur due to nonoptimal DGs allocation.

In the literature, many authors have discussed the use of different technologies to augment the performance of RDSs. The most effective techniques are system reinforcement/reconfiguration or integration of RDSs with DGs, SCBs, VRs, and sometimes their combination. However, most of the authors were much more
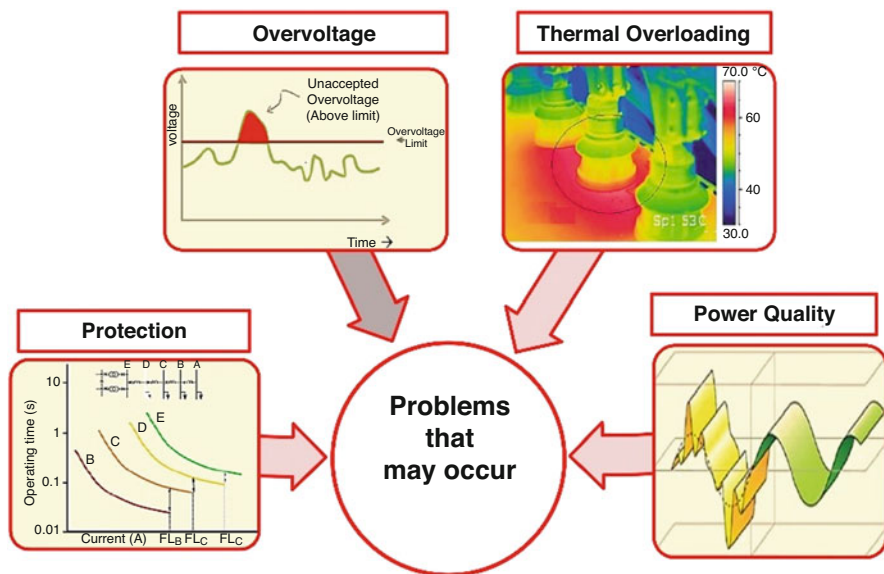

Fig. 2 Major problems that can occur with non-suitable DG ratings or locations

attentive to solving the optimal allocation problems of DGs or SCBs, either simultaneously or individually.

Khatod et al. in [10] used an evolutionary programming algorithm for power loss reduction and voltage profile improvement using optimally allocated DGs in RDSs. In [11], Muttaqi et al. presented an analytical (mathematical-based) approach that depends on algebraic equations to solve the optimal allocation problem of DGs to retain the RDSs' bus voltages within the specified permissible bounds. In [12], Ghanbari et al. applied particle swarm optimization to find DGs' size and optimal location in RDSs to minimize costs and reduce power losses. In [13], Ismael et al. used the crow search algorithm to allocate three DG types in RDS using a loss sensitivity index to choose the most candidate nodes for DG placement. In [14], Abdel-Mawgoud et al. employed a salp swarm algorithm to fit DGs to reduce energy losses in RDSs, while accounting for annual load growth. However, an economic cost model was not formulated in work.

Regarding SCBs allocation in the literature, many optimization procedures, such as particle swarm optimization [15], convex quadratic relaxations for mixed-integer nonlinear programs [16], differential evolution (DE) [17] and fuzzy-DE [18], ETAP tool [19], genetic algorithms [20] and others [21, 22], have been independently functioned for stand-alone SCBs allocation issues. However, it was evidenced that synchronized optimal allocation of SCBs and DGs in RDSs can accomplish better outcomes [23]. At the beginning of solving the problem, few researchers have focused on their simultaneous solution, but later this tendency becomes much more prominent.

In [24], Moradi et al. used a hybrid genetic-imperialist-competitive algorithm to solve the optimal allocation problem of DGs and SCBs to increase power loss reduction capability and enhance voltage regulation and voltage stability (VS).

In [25], Rahmani-Andebili resolved the same problem by employing genetic algorithms in RDSs from a distribution company's viewpoint to minimize total costs. In [26], Muthukumar and Jayalalitha presented a hybridization between harmony search and particle artificial bee colony algorithms to enhance VS and reduce losses by finding the optimal DGs and SCBs locations in RDSs. In [27], Yazdavar et al. determined the candidate sizes, places, and types of DGs and SCBs, in the planning phase in isolated microgrids (µGs) with the presence of nonlinear harmonic loads. In [28], Elattar et al. used an improved Manta-ray foraging optimization algorithm to synchronize DGs and SCBs in RDSs to diminish the unexploited consumed energy while satisfying the consumers' requirements. In [29], Kumar et al. joined the firefly and the backtracking algorithms to solve the DGs and SCBs allocation problem to diminish power loss and enhance the steady-state voltage profiles of the nodes in RDSs. In [30], Gampa and Das proposed a two-level multi-objective (MO) fuzzy-based grasshopper optimization procedure for allocating SCBs, DGs, and electric vehicle (EV) charging stations in RDSs, taking into account different technical QoP performance metrics. A genetic algorithm was also employed by Das et al. in [31] to distribute DGs and SCBs on the system relying on advancing voltage profile, reducing the current taken from the grid, and diminishing the power losses and annualized consumed energy.

Moreover, in [32], Almabsout et al. employed an enhanced GA to obtain optimal DGs and SCBs in small, medium, and large RDSs to diminish voltage deviation and power losses. In [33], Shaheen and El-Sehiemy introduced an optimally-coordinated allocation problem of DGs, SCBs, and VRs in RDSs and offered its solution using an adopted grey wolf algorithm. The results in that work confirmed that the used algorithm outperformed the other investigated algorithms regarding power losses, loading capacity, and voltage deviation reduction. Due to enlarged nonlinear loads usage and inverter-based DGs that cause harmonic distortion in RDSs, in [17], Milovanovich et al. allocated inverter-based DGs and SCBs using an improved hybrid particle-swarm-gravity-search algorithm to reduce energy losses.

Regarding VRs, the authors in [34] presented a computerized algorithm for optimal voltage control with VRs to reduce the cost of investing and the cost of energy losses. Also, in [35], a procedure for optimal sizing and siting of VRs has been presented to improve voltage profiles in RDSs. Other works introduced solutions for the optimal allocation of DGs or SCBs separately. Also, the optimal synchronization issue of DGs and VRs was explained in [36–38] and others for power loss minimization, voltage profile control, and VS enhancement. Finally, multi-agents (DGs, SCBs/SVC, or VRs) allocation to improve RDSs performance were presented in [33, 39], accounting for different QoP metrics using ETAP, MATLAB, GAMS [25], and others. However, economic considerations were not usually taken into account.

To sum up, improving the performance of RDSs is a primary target for power system operators. Besides, energy resource limitations and cost-effective electricity distribution to the consumers encourage engineers, distribution system operators, and researchers to investigate increasing the efficiency of electric power distribution systems. Fortunately, many technologies can effectively make such improvements. Active and reactive power compensators such as DGs and SCBs are examples of compensators that can effectively improve modern RDSs. VRs can also help these compensators function better in a much more effective techno-economic manner in RDSs and effectively enhance voltage profiles and load stability and reduce voltage deviations from the acceptable values. Unfortunately, rising project investment may result if uneconomic facilities or expensive technologies are used to reduce electric losses significantly. Therefore, economic considerations related to the installed network equipment should be considered. Also, it is clear from previous studies that no particular optimization method has proved to be the most appropriate method in the synchronized allocation of DGs, VRs, and SCBs objectives, and no guarantee of global solutions for different systems is evidenced.

Finally, to go over the main points, one can find that the standard objective functions in the allocation problem of active and reactive power conditioners and VRs are (i) power/energy loss reduction, (ii) voltage profile enhancement or voltage regulation adjustment or voltage deviation minimization, (iii) VS improvement, (iv) loading capacity/overloading minimization, (v) investment and operating cost minimization, (vi) power factor (PF) maximization, (vii) reducing the purchased apparent power from the electric utility/releasing the transformer capacity, and (viii) harmonic distortion mitigation. These different areas are explored in Fig. 3. Besides,
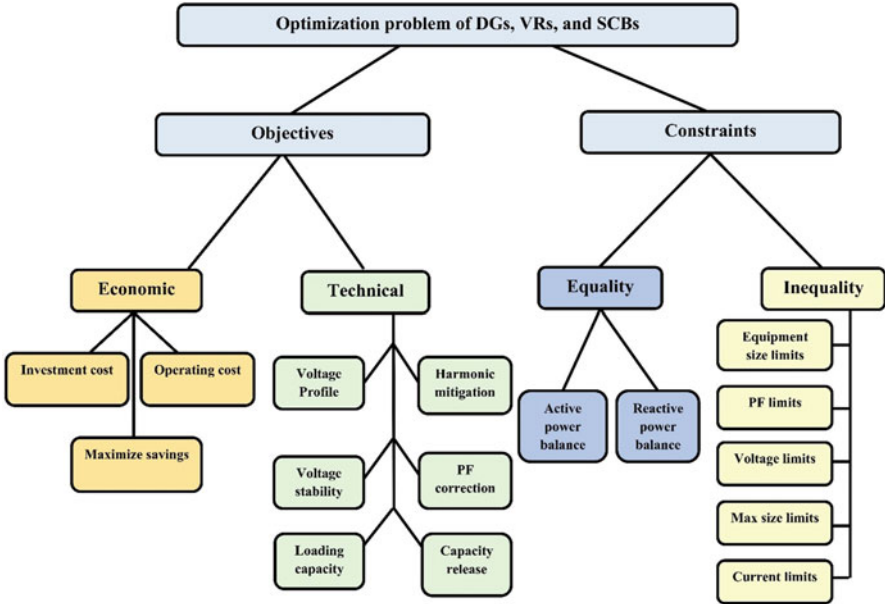
Fig. 3 Typical objectives and constraints used in DGs, VRs, and SCBs allocation

the typical constraints commonly considered (equality and inequality constraints) are explored in the figure. It should be noted that the harmonic mitigation goal is considered in case the loads are nonlinear harmonics-generating loads.

At the local level, to encounter the increasing load growth and hurrying too much to higher levels of mixed variable renewable energy sources (VRESs) integration, Egypt has established a promising energy strategy until 2035 to spread the power generation mix among fossil fuel-based plants. Therefore, improving the quality of power (QoP) performance levels of RDSs has become an authoritative area for system operators to host the ambitious number of renewables. In 2035, the growth of electricity demand will be satisfied in the "most likely" scenario by a combination of coal (48%), nuclear (8%), gas/oil-fired plants (22%), hydro (3%), wind (13%), photovoltaic (PV) (4%), and concentrated solar power (2%) [40]. However, Egypt faces abundant challenges – renewal of the existing deteriorated power generation plants, upgrade and development of transmission networks, dealing with the technical and nontechnical losses, pushing direction to use to the automated substation systems rather than the manual traditional operated substations, refining the energy laws to be more attractive for foreign investments, and the high spinning reserve that needs either interconnection with other countries or exporting electric energy to near countries.

In 2020, an increase in demand for investment in renewable energy was seen for both wind and solar energy projects. Many renewable energy projects have been implemented in Egypt to target 20% of the total energy produced in 2022. Egypt's total installed renewable energy capacity is 3.7 GW, including 2.8 GW of hydropower and about 0.9 GW of solar and wind power. In addition, the Egyptian

Table 1 Energy potential in Egypt by 2022 and 2035 [40]

Generation technology		In 2022 (short-term scenario)		In 2035 (long-term scenario)	
		Total share (%)	Share of each type (%)	Total share (%)	Share of each type (%)
Thermal power plants		80.00		55.00	
Renewable energy	Hydropower	20.00	6.00	42.00	2.00
	Solar energy		2.00		25.00
	Wind energy		12.00		15.00
	Nuclear energy	0.00	0.00	3.00	3.00

government has set renewable energy targets of 20% of the electricity mix by 2022 and 42% by 2035, as presented in Table 1 [40]. Egypt recommends key measures to accelerate renewables hosting [40] – power and energy sector strategies update to follow the rising benefits of renewable energy; biomass energy promotion in future energy strategy updates; reformation of the current market framework to improve project finance sources; universalization of regulations and explanation of institutional roles and responsibilities for wind and solar energy development; promotion of renewables and ensuring their financial viability; risk mitigation by proper solutions; the accomplishment of comprehensive measurement campaigns for solar and wind powers; and development of a dominant plan to boost local manufacturing capabilities to create a local renewable energy industry.

Accordingly, in this work, the well-known whale optimization algorithm (WOA) is applied in this work to allocate DGs, SCBs, and VRs in a realistic 37-bus distribution system in Egypt to minimize power losses while conforming with several linear and nonlinear constraints. A cost-benefit analysis of the optimization problem is made in terms of – investment and running costs of the compensators used, saving gained from the power loss reduction, and benefits from decreasing the power to be purchased from the grid, reducing voltage deviations and overloading, and enhancing VS. Three loading scenarios are considered in this work – light, shoulder, and peak levels of load demand. The numerical findings obtained show a noteworthy techno-economic improvement of the QoP performance level of the RDS and approve the efficiency and economic benefits of the proposed solutions compared to other solutions in the literature. Figure 4 displays a visualization of the compensators/considerations investigated in this work.

The rest of the chapter is arranged as follows: Sect. 2 presents the VS definition and the formulation used in this work. The VR model and its mathematical formulation are given in Sect. 3. Section 4 presents the load flow method used with and without the engaged VRs. Section 5 introduces the optimization problem and is investigated in detail. Section 6 explores the applied optimization method (WOA). Section 7 explores the metrics and indices used to qualify the performance of the system. Section 8 explores the system under study. Section 9 shows the results obtained, and their discussions are presented in the same section. Lastly, conclusions and future works are given in Sect. 10.
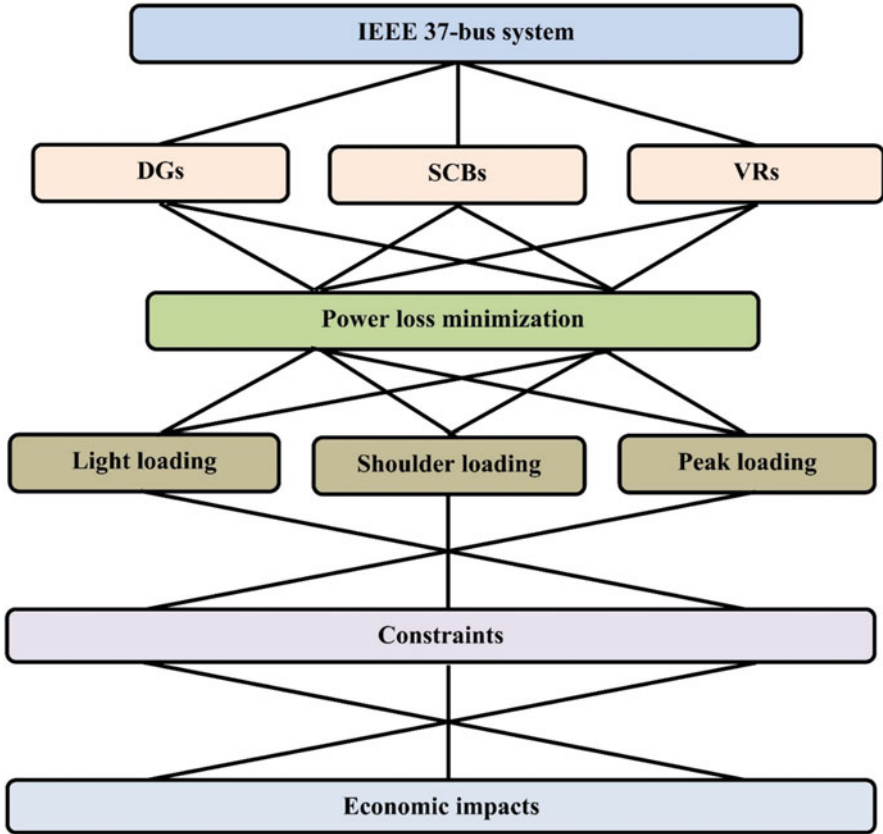
Fig. 4 Visualization of the compensators/considerations investigated in this work

2 Voltage Stability Analysis

Voltage stability (VS) analysis evaluates unstable or weak areas of electrical power systems that may endanger load growth due to unpredicted voltage collapse, and this means that operative VS analysis is essential in power system planning (PSP) and longstanding operability. In this regard, the authors in [41] proposed a voltage sensitivity analysis method that computes a metric at each bus to recognize the most sensitive bus for voltage collapse. The index is derived from a bi-quadratic expression usually employed in optimal power flow (OPF) algorithms [42].

For the explanatory distribution system model shown in Fig. 5. The quadratic expression relating the voltage magnitude at the sending and receiving nodes of a branch and power (active and reactive) at the receiving end is given as follows:
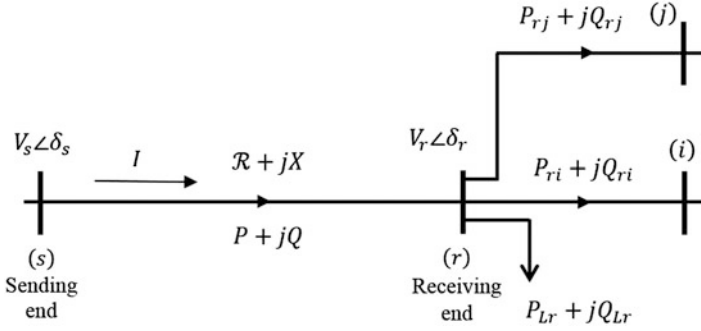
Fig. 5 Demonstrative distribution system model used in derivations

The line current (I) is stated as:

$$I = \frac{P - jQ}{V_r^*} \tag{1}$$

The sending-end voltage (V_s) is expressed as:

$$V_s = V_r + I\,(R + jX) \tag{2}$$

Combining these Eqs. (1) and (2), one can get the following:

$$V_s^2 = V_r^2 + 2\,(RP + XQ) + \left(R^2 + X^2\right)\left[\frac{P^2 + Q^2}{V_r^2}\right] \tag{3}$$

where V_s, V_r, $R + jX$, and $P + jQ$ denote the sending-end voltage, the receiving-end voltage, the impedance of the line, and the transferred active and reactive power, respectively.

Multiplying Eq. (3) by (V_r^2) will lead to the well-known expression in Eq. (4):

$$V_r^2 V_s^2 = V_r^4 + 2\,(RP + XQ)\,V_r^2 + \left(R^2 + X^2\right)\left(P^2 + Q^2\right)$$

$$\Rightarrow V_r^4 - \left[V_s^2 - 2\,(RP + XQ)\right]V_r^2 + \left[\left(R^2 + X^2\right)\left(P^2 + Q^2\right)\right] = 0 \tag{4}$$

$$\Rightarrow a V_r^4 - b V_r^2 + c = 0$$

so that:

$$\begin{aligned}
a &= 1\\
b &= V_s^2 - 2\,(RP + XQ)\\
c &= \left(R^2 + X^2\right)\left(P^2 + Q^2\right)
\end{aligned} \tag{5}$$

It is clear from (5) that the solution of the equation will provide four roots, and only the maximum positive roots are the feasible solutions that will give the V_r values. Thus:

$$V_r = \frac{1}{\sqrt{2}}\sqrt{\left(b + \left(\sqrt{b^2 - 4c}\right)\right)} \tag{6}$$

The critical loading point or voltage instability or collapse will not be reached if Eq. (7) is satisfied.

$$b^2 - 4c \geq 0$$
$$\Rightarrow \left[V_s^2 - 2\,(RP + XQ)\right]^2 - 4\left(R^2 + X^2\right)\left(P^2 + Q^2\right) \geq 0 \tag{7}$$

This will lead to the following:

$$V_s^4 - 4(PX - QR)^2 - 4V_s^2\,(PR + QX) \geq 0 \tag{8}$$

The voltage stability index (VSI) can be expressed as follows:

$$VSI_{bus} = V_s^4 - 4(PX - QR)^2 - 4V_s^2\,(PR + QX)\,, \forall bus \tag{9}$$

The low values of VSI_{bus} correspond to a much higher possibility of voltage instability or extreme voltage collapse, as illustrated in Fig. 6. Voltage collapse (VC)
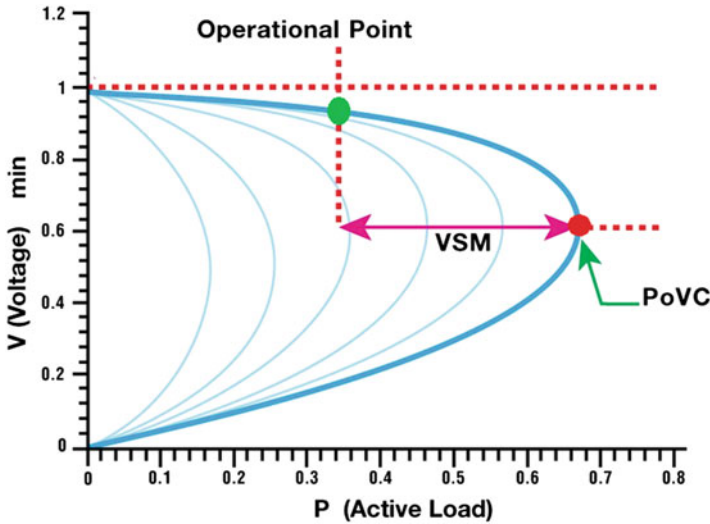
Fig. 6 Illustration of the VSM concept on an illustrative PV curve from ETAP voltage stability software

becomes much more probable when the power system operates with an insufficient VS margin (VSM) in at least one bus. *VSM* is the distance between the current operating point and the collapse point (PoVC). Periodic studies must be performed to decide if the grid is susceptible to VC and find proper solutions to avoid it, predominantly, under heavily loaded conditions.

3   Voltage Regulators

Supplying every customer with a voltage within acceptable limits is an essential distribution feeder requirement; thus, the voltages should be regulated. VR is one of the most common ways used. An automatic VR comprises an autotransformer and a load tap shifting mechanism that tolerates handling the tap location, in which the output voltage can be adjusted by varying the tap location through changing the winding (series-winding of the autotransformer).

   The control circuit, known as the line drop compensator, governs the tap location [43]. Step VRs can be connected as Type A or Type B connections, reported in ANSI/IEEE C57.15 standard series [44] that classifies the voltage ranges in these types. However, Type B-VR is more common. Figure 7 illustrates a schematic diagram of a step VR in the raise position [45].
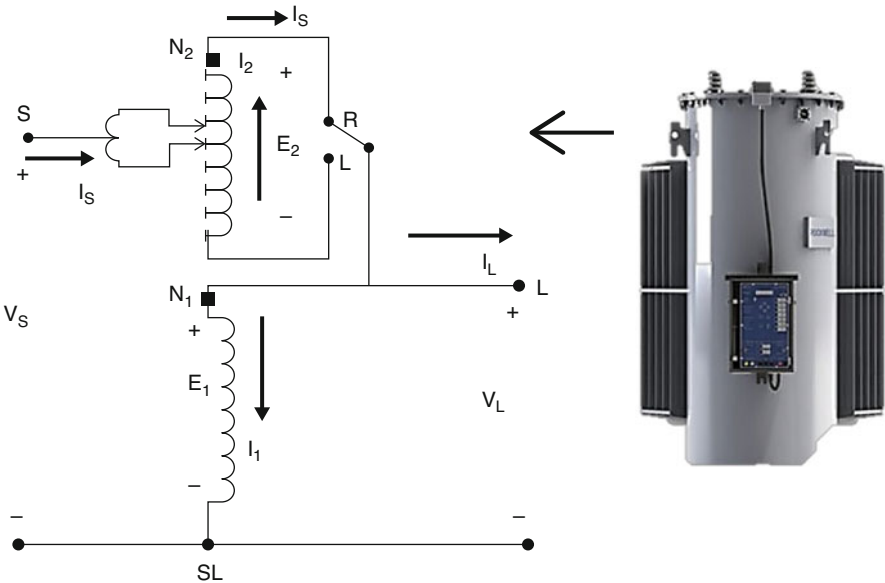
Fig. 7 Diagram of a step VR, Type B

A standard step VR comprises a reversing switch that allows the voltage to be regulated in a range of $\pm 10\%$ of the rated voltage, up and down. Characteristically, the voltage is stepped in 8, 16, or 32 steps. The 32-step is the most common in substations (16 in the up-voltage raise position and 16 in the down-voltage lower position). Each step change is equivalent to a 0.00625 per unit change in the voltage (each change in tap changes the voltage by (5/8) % or 0.00626 per unit to give the $\pm 10\%$ of the rated voltage). VRs may connect as Y or $\Delta$ or open Δ for a three-phase system. Bandwidth is always set so that the taps are only changed when the voltage is out of the bandwidth. It is specified by minimum and maximum regulation voltage (set to $\pm 1\%$ of the nominal voltage) to bound the number of changes of the tapping.

The mathematical description of a phase VR is formulated as follows:

$$V_S = a_R V_L, \ I_L = a_R I_S \tag{10}$$

where V_S denotes the supply voltage, V_L denotes the load voltage, and a_R denotes the effective VR ratio, which can be defined in terms of the transformer turns ratio as follows:

$$a_R = \begin{cases} 1 - \frac{N_2}{N_1}, \text{ raise position} \\ 1 + \frac{N_2}{N_1}, \text{ lower position} \end{cases} \tag{11}$$

Additionally, the effective regulator ratio can be defined in terms of the tap position (TP) as follows:

$$a_R = \begin{cases} 1 - (0.00625 \times \text{TP}), \text{ raise position} \\ 1 + (0.00625 \times \text{TP}), \text{ lower position} \end{cases} \tag{12}$$

One can refer to [45] to find more details on VRs and control circuits.

4 Optimal Power Flow (OPF)

Due to the RDSs topology, the OPF-based matrices presented in [46] were used in work done in this chapter. It relies on three matrices – the bus-injection-to-branch-current matrix, designated as [BIBC], the branch-current-to-bus-voltage matrix, specified as [BCBV], and their multiplication matrix [CV] to solve the OPF problem. This matrices method is effective and efficient in solving OPF in RDSs. First of all, let us define an illustrative nine-bus RDS, shown in Fig. 8. BC_i represents the ith branch current, and I_i represents the ith bus injection current, where i represents the bus number. At each i, one can compute the complex apparent load power (S_i), as follows:

$$S_i = P_i + jQ_i, \forall i \in n \tag{13}$$
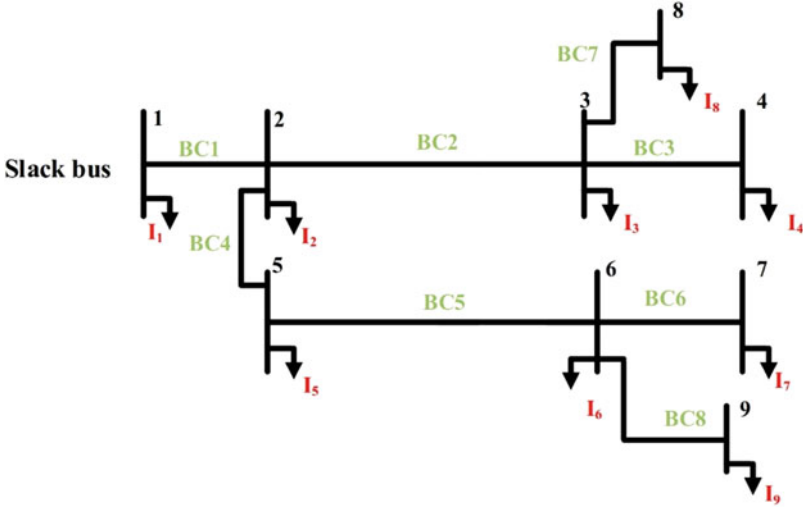
Fig. 8 A simple nine-bus RDS

where P_i and Q_i denote the active and reactive load power at bus i, respectively, and n represents the total bus number, i.e., $n = 9$. The current injection at iteration (itr) is specified using P_i, Q_i, and the ith bus voltage, V_i, as follows:

$$I_i^{\text{iter}} = \left(\frac{P_i + jQ_i}{V_i^{\text{itr}}} \right)^*, \forall i \in n, \forall \text{itr} \in \text{itr}_{\max} \tag{14}$$

The iteration number (itr) should be less than or equal to the maximum iteration number specified ($\text{itr}_{\max}$), i.e., $\text{itr} \leq \text{itr}_{\max}$. Hereafter, using Eq. (14), equivalent bus current injections are obtained. Further, the branch currents can be computed from Kirchhoff's current law applied to RDS, as shown in Eq. (15). Then, one can formulate the relation between the branch and load currents and put it in the matrix form, as follows:

$$
\begin{aligned}
BC_8 &= I_9 \\
BC_7 &= I_8 \\
BC_6 &= I_7 \\
BC_5 &= I_6 + BC_6 + BC_8 = I_6 + I_7 + I_9 \\
BC_4 &= I_5 + BC_5 = I_5 + I_6 + I_7 + I_9 \\
BC_3 &= I_4 \\
BC_2 &= I_3 + BC_3 + BC_7 = I_3 + I_4 + I_8 \\
BC_1 &= I_2 + BC_2 + BC_4 = I_2 + I_3 + I_4 + I_5 + I_6 + I_7 + I_8 + I_9
\end{aligned}
\tag{15}
$$

$$\begin{bmatrix} BC_1 \\ BC_2 \\ BC_3 \\ BC_4 \\ BC_5 \\ BC_6 \\ BC_7 \\ BC_8 \end{bmatrix} = \begin{bmatrix} 1\ 1\ 1\ 1\ 1\ 1\ 1\ 1 \\ 0\ 1\ 1\ 0\ 0\ 0\ 1\ 0 \\ 0\ 0\ 1\ 0\ 0\ 0\ 0\ 0 \\ 0\ 0\ 0\ 1\ 1\ 1\ 0\ 1 \\ 0\ 0\ 0\ 0\ 1\ 1\ 0\ 1 \\ 0\ 0\ 0\ 0\ 0\ 1\ 0\ 0 \\ 0\ 0\ 0\ 0\ 0\ 0\ 1\ 0 \\ 0\ 0\ 0\ 0\ 0\ 0\ 0\ 1 \end{bmatrix} \times \begin{bmatrix} I_2 \\ I_3 \\ I_4 \\ I_5 \\ I_6 \\ I_7 \\ I_8 \\ I_9 \end{bmatrix} \quad (16)$$

Equation (16) can be generalized to be in terms of [BIBC], as follows:

$$[BC] = [BIBC] \times [I] \quad (17)$$

The ith bus voltage can be obtained from Kirchhoff's voltage law applied to RDS; as follows:

$$
\begin{aligned}
cV_2 &= V_1 - BC_1 Z_{12} \\
V_3 &= V_2 - BC_2 Z_{23} = V_1 - BC_1 Z_{12} - BC_2 Z_{23} \\
V_4 &= V_3 - BC_3 Z_{34} = V_1 - BC_1 Z_{12} - BC_2 Z_{23} - BC_3 Z_{34} \\
V_5 &= V_2 - BC_4 Z_{25} = V_1 - BC_1 Z_{12} - BC_4 Z_{25} \\
V_6 &= V_5 - BC_5 Z_{56} = V_1 - BC_1 Z_{12} - BC_4 Z_{25} - BC_5 Z_{56} \\
V_7 &= V_6 - BC_6 Z_{67} = V_1 - BC_1 Z_{12} - BC_4 Z_{25} - BC_5 Z_{56} - BC_6 Z_{67} \\
V_8 &= V_3 - BC_7 Z_{38} = V_1 - BC_1 Z_{12} - BC_2 Z_{23} - BC_7 Z_{38} \\
V_9 &= V_6 - BC_8 Z_{69} = V_1 - BC_1 Z_{12} - BC_4 Z_{25} - BC_5 Z_{56} - BC_8 Z_{69}
\end{aligned}
\quad (18)
$$

Z_{ij} denotes the impedance between buses i and j. From Eq. (18), V_i is formulated in terms of BCs, Z_{ij}, and the slack bus or substation voltage (V_1). Therefore, the connection between BCs and V_{is} can be stated as follows:

$$\begin{bmatrix} V_2 \\ V_3 \\ V_4 \\ V_5 \\ V_6 \\ V_7 \\ V_8 \\ V_9 \end{bmatrix} = \begin{bmatrix} V_1 \\ V_1 \\ V_1 \\ V_1 \\ V_1 \\ V_1 \\ V_1 \\ V_1 \end{bmatrix} - \begin{bmatrix} Z_{12} & 0 & 0 & 0 & 0 & 0 & 0 & 0 \\ Z_{12} & Z_{23} & 0 & 0 & 0 & 0 & 0 & 0 \\ Z_{12} & Z_{23} & Z_{34} & 0 & 0 & 0 & 0 & 0 \\ Z_{12} & 0 & 0 & Z_{25} & 0 & 0 & 0 & 0 \\ Z_{12} & 0 & 0 & Z_{25} & Z_{56} & 0 & 0 & 0 \\ Z_{12} & 0 & 0 & Z_{25} & Z_{56} & Z_{67} & 0 & 0 \\ Z_{12} & Z_{23} & 0 & 0 & 0 & 0 & Z_{38} & 0 \\ Z_{12} & 0 & 0 & Z_{25} & Z_{56} & 0 & 0 & Z_{69} \end{bmatrix} \times \begin{bmatrix} BC_1 \\ BC_2 \\ BC_3 \\ BC_4 \\ BC_5 \\ BC_6 \\ BC_7 \\ BC_8 \end{bmatrix}$$

$$(19)$$

Consequently, the voltage drops (ΔV) between each bus V_i and the slack bus V_1 is given as follows:

$$
\begin{bmatrix} V_1 \\ V_1 \\ V_1 \\ V_1 \\ V_1 \\ V_1 \\ V_1 \\ V_1 \end{bmatrix} - \begin{bmatrix} V_2 \\ V_3 \\ V_4 \\ V_5 \\ V_6 \\ V_7 \\ V_8 \\ V_9 \end{bmatrix} = \begin{bmatrix} Z_{12} & 0 & 0 & 0 & 0 & 0 & 0 & 0 \\ Z_{12} & Z_{23} & 0 & 0 & 0 & 0 & 0 & 0 \\ Z_{12} & Z_{23} & Z_{34} & 0 & 0 & 0 & 0 & 0 \\ Z_{12} & 0 & 0 & Z_{25} & 0 & 0 & 0 & 0 \\ Z_{12} & 0 & 0 & Z_{25} & Z_{56} & 0 & 0 & 0 \\ Z_{12} & 0 & 0 & Z_{25} & Z_{56} & Z_{67} & 0 & 0 \\ Z_{12} & Z_{23} & 0 & 0 & 0 & 0 & Z_{38} & 0 \\ Z_{12} & 0 & 0 & Z_{25} & Z_{56} & 0 & 0 & Z_{69} \end{bmatrix} \times \begin{bmatrix} BC_1 \\ BC_2 \\ BC_3 \\ BC_4 \\ BC_5 \\ BC_6 \\ BC_7 \\ BC_8 \end{bmatrix}
$$

$$(20)$$

Equation (20) can be generalized to be in terms of [BCBV], as follows:

$$[\Delta V] = [BCBV] \times [BC] \tag{21}$$

Combining Eqs. (17) and (21), the relationship between I_{is} and V_{is} can be expressed as follows:

$$[\Delta V] = [BCBV] \times [BC] = [BCBV] \times [BIBC] \times [I] \tag{22}$$

$$[\Delta V] = [CV] \times [I] \tag{23}$$

[CV] is a multiplication matrix of [BCBV] and [BIBC] matrices. The dimension of [BIBC] is $m \times (n-1)$, where m is the number of branches, and the size of [BCBV] is $(n-1) \times m$. [CV] is given as follows:

$$[CV] = [BCBV] \times [BIBC] \tag{24}$$

The OPF solution for RDS can be obtained by solving the following equations iteratively, at itr $\in$ itr$_{max}$; thus:

$$I_i^{itr} = \left(\frac{P_i + jQ_i}{V_i^{itr}} \right)^*, \forall i \in n, \forall itr \in itr_{max} \tag{25}$$

$$\Delta V_i^{itr+1} = [CV] \times I_i^{itr}, \forall i \in n, \forall itr \in itr_{max} \tag{26}$$

$$V_i^{itr+1} = V_i^{itr} + \Delta V_i^{itr+1}, \forall i \in n, \forall itr \in itr_{max} \tag{27}$$
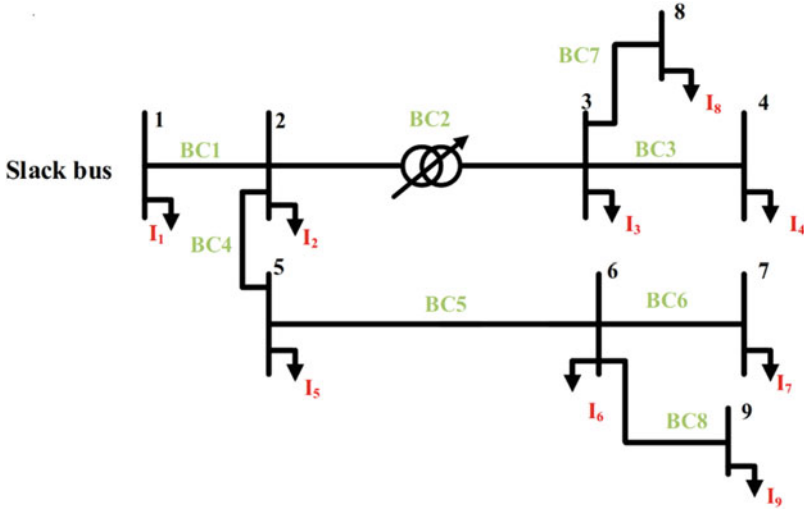
Fig. 9 Adopted nine-bus RDS with VR included in the system

A modified mathematical-based OPF technique for RDSs with VRs embedded in the system is presented to provide the load flow and VR's optimum tap setting as quickly as possible.

To demonstrate the updated OPF procedure, the nine-bus RDS is modified to include a VR between bus #2 and bus #3, as shown in Fig. 9.

One can formulate the branch and load currents and put them in matrix form, as follows:

$$BC_8 = I_9$$

$$BC_7 = I_8$$

$$BC_6 = I_7$$

$$BC_5 = I_6 + BC_6 + BC_8 = I_6 + I_7 + I_9$$

$$BC_4 = I_5 + BC_5 = I_5 + I_6 + I_7 + I_9 \tag{28}$$

$$BC_3 = I_4$$

$$BC_2 = \frac{I_3}{a_R} + \frac{BC_3}{a_R} + \frac{BC_7}{a_R} = \frac{I_3}{a_R} + \frac{I_4}{a_R} + \frac{I_8}{a_R}$$

$$BC_1 = I_2 + BC_2 + BC_4 = I_2 + \frac{I_3}{a_R} + \frac{I_4}{a_R} + I_5 + I_6 + I_7 + \frac{I_8}{a_R} + I_9$$

Then;

$$
\begin{bmatrix} BC_1 \\ BC_2 \\ BC_3 \\ BC_4 \\ BC_5 \\ BC_6 \\ BC_7 \\ BC_8 \end{bmatrix} = \begin{bmatrix} 1 & \frac{1}{a_R} & \frac{1}{a_R} & 1 & 1 & 1 & \frac{1}{a_R} & 1 \\ 0 & \frac{1}{a_R} & \frac{1}{a_R} & 0 & 0 & 0 & \frac{1}{a_R} & 0 \\ 0 & 0 & 1 & 0 & 0 & 0 & 0 & 0 \\ 0 & 0 & 0 & 1 & 1 & 1 & 0 & 1 \\ 0 & 0 & 0 & 0 & 1 & 1 & 0 & 1 \\ 0 & 0 & 0 & 0 & 0 & 1 & 0 & 0 \\ 0 & 0 & 0 & 0 & 0 & 0 & 1 & 0 \\ 0 & 0 & 0 & 0 & 0 & 0 & 0 & 1 \end{bmatrix} \times \begin{bmatrix} I_2 \\ I_3 \\ I_4 \\ I_5 \\ I_6 \\ I_7 \\ I_8 \\ I_9 \end{bmatrix} \tag{29}
$$

Also, the ith bus voltage equations and the branch current relations can be written as follows:

$$
\begin{aligned}
V_2 &= V_1 - BC_1 Z_{12} \\
V_3 &= \left(\frac{V_2 - BC_2 Z_{23}}{a_R} \right) = \frac{V_1 - BC_1 Z_{12} - BC_2 Z_{23}}{a_R} \\
V_4 &= V_3 - BC_3 Z_{34} = \frac{V_1 - BC_1 Z_{12} - BC_2 Z_{23}}{a_R} - BC_3 Z_{34} \\
V_5 &= V_2 - BC_4 Z_{25} = V_1 - BC_1 Z_{12} - BC_4 Z_{25} \\
V_6 &= V_5 - BC_5 Z_{56} = V_1 - BC_1 Z_{12} - BC_4 Z_{25} - BC_5 Z_{56} \\
V_7 &= V_6 - BC_6 Z_{67} = V_1 - BC_1 Z_{12} - BC_4 Z_{25} - BC_5 Z_{56} - BC_6 Z_{67} \\
V_8 &= V_3 - BC_7 Z_{38} = \frac{V_1 - BC_1 Z_{12} - BC_2 Z_{23}}{a_R} - BC_7 Z_{38} \\
V_9 &= V_6 - BC_8 Z_{69} = V_1 - BC_1 Z_{12} - BC_4 Z_{25} - BC_5 Z_{56} - BC_8 Z_{69}
\end{aligned} \tag{30}
$$

$$
\begin{bmatrix} V_2 \\ V_3 \\ V_4 \\ V_5 \\ V_6 \\ V_7 \\ V_8 \\ V_9 \end{bmatrix} = \begin{bmatrix} V_1 \\ V_1 / a_R \\ V_1 / a_R \\ V_1 \\ V_1 \\ V_1 \\ V_1 / a_R \\ V_1 \end{bmatrix} - [BCBV] \times \begin{bmatrix} BC_1 \\ BC_2 \\ BC_3 \\ BC_4 \\ BC_5 \\ BC_6 \\ BC_7 \\ BC_8 \end{bmatrix} \tag{31}
$$

so that:

$$[\text{BCBV}] = \begin{bmatrix} Z_{12} & 0 & 0 & 0 & 0 & 0 & 0 & 0 \\ Z_{12}/a_{\text{R}} & Z_{23}/a_{\text{R}} & 0 & 0 & 0 & 0 & 0 & 0 \\ Z_{12}/a_{\text{R}} & Z_{23}/a_{\text{R}} & Z_{34} & 0 & 0 & 0 & 0 & 0 \\ Z_{12} & 0 & 0 & Z_{25} & 0 & 0 & 0 & 0 \\ Z_{12} & 0 & 0 & Z_{25} & Z_{56} & 0 & 0 & 0 \\ Z_{12} & 0 & 0 & Z_{25} & Z_{56} & Z_{67} & 0 & 0 \\ Z_{12}/a_{\text{R}} & Z_{23}/a_{\text{R}} & 0 & 0 & 0 & 0 & Z_{38} & 0 \\ Z_{12} & 0 & 0 & Z_{25} & Z_{56} & 0 & 0 & Z_{69} \end{bmatrix} \tag{32}$$

Accordingly, one has to perform the OPF without VRs included. One VR is added to the system between two buses, and the minimum and maximum regulation voltage values are identified, a_{R} is initially set to 1 and TP_{old} is set to 0. If the voltage at the VR bus exceeds the maximum regulation voltage, then Eq. (33) is applied to lower the voltage.

$$\begin{aligned} \text{TP}_{\text{change}} &= \frac{V_{\text{VR}} - V_{\text{max}}}{0.00625}, \\ \text{TP}_{\text{new}} &= \text{TP}_{\text{old}} - \text{TP}_{\text{change}}, \forall \text{TP} = \{1, 2...16\} \\ a_{\text{R}} &= 1 + 0.00625 \, (\text{TP}_{\text{new}}) \end{aligned} \tag{33}$$

Otherwise, Eq. (34) is used to raise the voltage if the voltage at the VR bus is lower than the minimum voltage value.

$$\begin{aligned} \text{TP}_{\text{change}} &= \frac{V_{\text{min}} - V_{\text{VR}}}{0.00625}, \\ \text{TP}_{\text{new}} &= \text{TP}_{\text{old}} + \text{TP}_{\text{change}}, \forall \text{TP} = \{1, 2...16\} \\ a_{\text{R}} &= 1 - 0.00625 \, (\text{TP}_{\text{new}}) \end{aligned} \tag{34}$$

Iteratively, this will be repeated until no change occurs in the tap; $\text{TP}_{\text{new}} = \text{TP}_{\text{old}}$. Consequently, the procedure will be recurrent for all VRs connected to the system.

5   Formulation of the Problem

The objective function (f) formulated in this work minimizes the total active power losses ($P_{\text{loss,tot}}$) given in Eq. (35) in three equally weighted loading scenarios – light (Lig), shoulder (Sh), and peak (Pk) levels of load demand. k_1, k_2, and k_3 are the weighting factors of the loading scenarios.

$$f = \min P_{\text{loss,tot}} = \min_h (k_1 P_{\text{loss}}(\text{lig}) + k_2 P_{\text{loss}}(\text{Sh}) + k_3 P_{\text{loss}}(\text{Pk})), \, h = 8760 \tag{35}$$

Lig represents 60% of the peak loading level of hours, Sh represents 80% of the peak loading, and Pk represents 100%. Each of them occurs for 2920 hours per year. At that time, f subjects to a different set of constraints – equality power flow constraints represented by Eqs. (36) and (37), DGs size limits represented by (38), DGs penetration represented by (39), PF limits represented by (40), SCBs size represented by (41), the hth branch current thermal limits represented by (42), and the hth allowable voltage boundaries, represented by (43). The suffix min denotes the minimum value of the variable/parameter, while max denotes the maximum value of the variable/parameter.

$$P_{\text{grid}} + \sum_{g=1}^{N_{\text{DG}}} P_{\text{DG}}(g) = \sum_{i=1}^{n} P_{\text{d}}(i) + \sum_{\text{br}=1}^{N_{\text{br}}} P_{\text{loss}}\,(\text{br})\,, \forall g \in N_{\text{DG}}, \forall \text{br} \in N_{\text{br}}, \forall i \in n \tag{36}$$

$$Q_{\text{grid}} + \sum_{c=1}^{N_{\text{SCB}}} Q_{\text{SCB}}(c) = \sum_{i=1}^{n} Q_{\text{d}}(i) + \sum_{\text{br}=1}^{N_{\text{br}}} Q_{\text{loss}}\,(\text{br})\,, \forall c \in N_{\text{SCB}}, \forall \text{br} \in N_{\text{br}}, \forall i \in n \tag{37}$$

where P_{grid} and Q_{grid} denote the grid' active and reactive power, respectively, P_{loss} and Q_{loss} denote the active and reactive power losses, respectively, and $P_{\text{d}}\,(i)$ and $Q_{\text{d}}\,(i)$ denote the ith real and reactive power demand. N_{br} denotes the total number of branches, and n denotes the number of buses in the power system. N_{DG} and N_{SCB} denote the total number of DGs and SCBs, respectively, P_{DG} denotes the DG's active power, and Q_{SCB} denotes the SCB's reactive power.

$$P_{\text{DG}}(g) \leq P_{\text{DG}}(g)_{\max}, \forall g \in N_{\text{DG}} \tag{38}$$

$$\sum_{g=1}^{N_{\text{DG}}} P_{\text{DG}}(g) \leq \alpha \sum_{i=1}^{n} P_{\text{d}}(i), \forall g \in N_{\text{DG}} \tag{39}$$

In Eq. (39), α represents a percentage of the demand power in which the maximum permissible DG penetration is determined when one constraint violates the limit.

$$0.85\ \text{lag} \leq \text{PF} \leq 1 \tag{40}$$

$$Q_{\text{SCB}}(c) \leq Q_{\text{SCB}}(c)_{\max}, \forall c \in N_{\text{SCB}} \tag{41}$$

$$I_{\mathrm{br},h} \leq I_{\mathrm{max,br}}, \forall \mathrm{br} \in N_{\mathrm{br}}, \forall h \tag{42}$$

$$V_i^{\min} \leq V_{i,h} \leq V_i^{\max}, \forall i \in n, \forall h \tag{43}$$

6   Whale Optimization Algorithm (WOA)

Nature-inspired metaheuristic algorithms (NIMHAs) have amazingly solved complex engineering problems. In this realm, WOA is a population-based NIMHA settled by Mirjalili and Lewis in 2016, and it was grounded on imitating the pursuing behavior of a specific kind of the seven whale types called the humpback whale (HW) [47]. Whales, the largest mammals in the world, are brilliant emotional creatures. Whales have cells similar to those found in humans in their brains, so-called spindle cells, responsible for emotional actions, judgment, and social behaviors in general. The hunting method of HWs is termed the net-bubble feeding method (NBFM). HWs select to catch small fishes (as prey) near the surface [48].

When HW notices its prey, it dives about 12 m down and then begins to make spiral bubbles around the prey. The prey is afraid to cross these bubbles, which appear as a trap. Hence, HW swims up to the surface and collects its trapped prey, as illustrated in Fig. 10.

The NBFM of the HW is mathematically modeled in three phases – encircling preys, NBFM as the exploitation (EXPL) phase, and the exploration (EXPR) phase. The EXPL is also divided into the shrink mechanism and the spiral position's update [47].
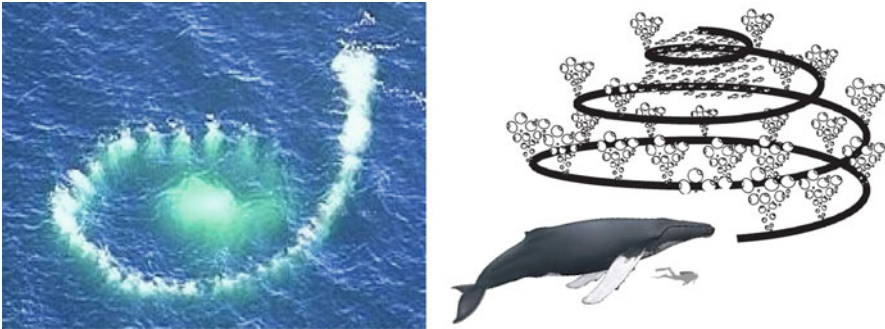
Fig. 10 Net-bubble trap of the HWs during hunting

6.1 Encircling Stage

HWs can recognize and surround the prey's location. Since the optimal design position in the search space is unknown, the WOA considers the current search factor as the target prey (or solution) or close to the optimal one.

After the best search representative is defined, other search representatives try to update their location toward the best search representative, as represented by the following equations: t denotes the current iteration, $t + 1$ denotes the subsequent iteration to t, X^* denotes the position vector of the best solution obtained. It is iteratively updated until the best value is obtained or the maximum iterations number, t_{max}, is reached and $\overrightarrow{X}$ denotes the position vector. | | indicates the absolute value (abs), and $\cdot$ means multiplication.

$$\overrightarrow{D} = \left| \overrightarrow{C} \cdot \overrightarrow{X}^*(t) - \overrightarrow{X}(t) \right| \tag{44}$$

$$\overrightarrow{X}(t + 1) = \overrightarrow{X}^*(t) - \overrightarrow{A} \cdot \overrightarrow{D} \tag{45}$$

The vectors $\overrightarrow{A}$ and $\overrightarrow{C}$ are formulated as follows:

$$\overrightarrow{A} = 2\left(\overrightarrow{a} \cdot \overrightarrow{r}\right) - \overrightarrow{a} \tag{46}$$

$$\overrightarrow{C} = 2\overrightarrow{r} \tag{47}$$

where $\overrightarrow{a}$ is promoted to linearly decrease from 2 to 0 to characterize the spiral bubbles over the iterations and $\overrightarrow{r}$ denotes a random vector that ranges between [0,1]. $\overrightarrow{D}$ denotes the abs difference between the obtained solutions.

6.1.1 Bubble-Net Hunting Stage

Shrink Mechanism
This mechanism is realized by decreasing $\overrightarrow{a}$ shown in Eq. (46) from 2 to 0. This, in turn, decreases $\overrightarrow{A}$'s value in a random manner in $[-a, a]$. Figure 11 illustrates the possible positions of random HW's at (X, Y) toward the prey at (X^*, Y^*), keeping that $(0 \leq A \leq 1)$.
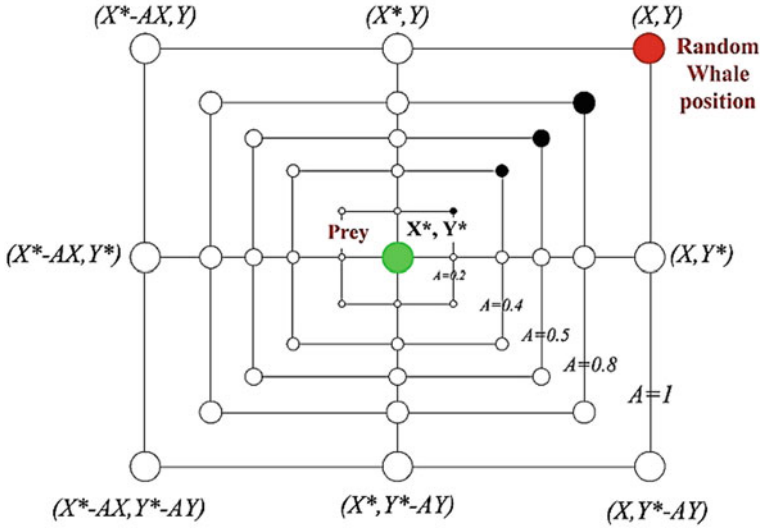
Fig. 11 Illustration of the shrink mechanism

Spiral Update (Helix-Based Movement)

The distance between the HW at (X, Y) and the prey at (X^*, Y^*) is computed first. At that point, a spiral mechanism is created between the HW's and prey's positions to imitate a helix-based movement as explored in Fig. 12.

$$\overrightarrow{X}(t+1) = \overrightarrow{D}' . e^{sl} . \cos(2\pi l) + \overrightarrow{X}^*(t) \tag{48}$$

$$\overrightarrow{D}'_i = \left| \overrightarrow{X}^*(t) - \overrightarrow{X}(t) \right| \tag{49}$$

where $\overrightarrow{D}'_i$ denotes the distance between an ith HW and the prey, s represents the shape of the logarithmic spiral, l is a random number in $[-1,1]$.

The HWs swim around the prey using the shrink mechanism or along a spiral-shaped path. Mathematically, a 50% probability is assumed in the optimization process to choose either shrinking or spiral moving toward the prey in updating the HWs' position. Thus;

$$\overrightarrow{X}(t+1) = \begin{cases} \overrightarrow{X}^*(t) - \overrightarrow{A} . \overrightarrow{D}, & \forall \ p_r < 0.5 \\ \overrightarrow{X}(t+1) = \overrightarrow{D}' . e^{sl} . \cos(2\pi l) + \overrightarrow{X}^*(t) & \forall \ p_r \geq 0.5 \end{cases} \tag{50}$$

where p_r denotes a random number in $[0,1]$.

Fig. 12 Illustration of the spiral update mechanism
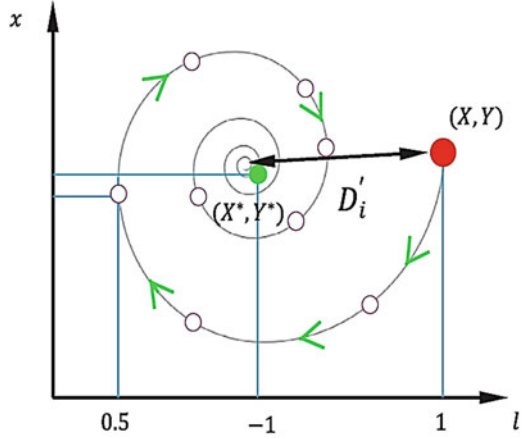
Table 2 The values of the parameters used

Parameter	Value
Number of search agents	30
$\vec{a}$	Linearly decreases from 2 to 0
Maximum number of iterations	2000

6.1.2 Exploration (EXPR) Stage

The vector $\vec{A}$ with random values greater than 1 or less than -1, $\left|\vec{A}\right| > 1$, was employed to force search agents to move far away from a reference HW to avoid interactions between them during hunting. Besides, the HWs (search agents) search for the best prey (global solution) randomly and change their positions according to the position of other HWs. To consider this randomness, Eqs. (44) and (45) are updated after replacing X^* with $\vec{X}_{\text{rand}}$, where $\vec{X}_{\text{rand}}$ is a random position vector (a random HW) chosen from the population. as follows:

$$\vec{D} = \left|\vec{C}.\vec{X}_{\text{rand}}(t) - \vec{X}(t)\right| \tag{51}$$

$$\vec{X}(t+1) = \vec{X}_{\text{rand}}(t) - \vec{A}.\vec{D} \tag{52}$$

To recap, the WOA parameters used in this work are given in Table 2, and the WOA's flowchart is shown in Fig. 13.
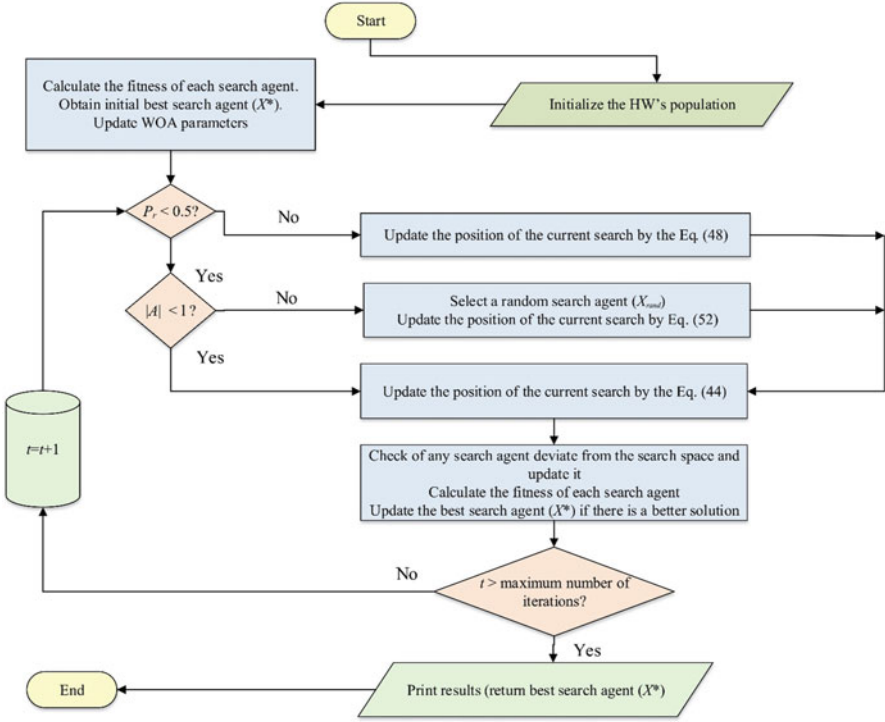
Fig. 13 Flowchart for WOA

7 Qualification of the Performance of the System

The different metrics and indices used to qualify the studied system's performance and determine the economic benefits are presented in this section.

7.1 Technical Indices

Reduction in the Active Energy Loss Benefits (TI$_P$)
The difference in the active energy loss values before and after compensation, \$/year, is formulated in (53), where R_1 represents the tariff rate of the energy (\$/kWh), and s denotes the scenario number. R_1 equals \$0.06/kWh as given in [33, 49].

$$\text{TI}_P = \sum_{s=1}^{s=3} \left[R_1 h \left(P_{\text{loss},s}^{\text{before}} - P_{\text{loss},s}^{\text{after}} \right) \right], s \in \{\text{Lig, Sh, Pk}\} \tag{53}$$

Reduction in the Apparent Power Purchased from the Grid (TI_S)

The change in the contracted apparent power (*Sgrid*) values before and after compensation, \$/year, is formulated in (54), where R_2 represents the tariff rate of the apparent power (\$/kVAh) and is set to \$0.06/kWh [33, 49].

$$TI_S = \sum_{s=1}^{s=3} \left[R_2 \left(S_{grid,s}^{before} - S_{grid,s}^{after} \right) \right], s \in \{Lig, Sh, Pk\} \tag{54}$$

Enhancement of the Voltage Profile (TI_{VD})

The voltage profile enhancement is formulated by calculating the sum of the absolute values of the squared voltage of each bus deviated from one per unit at the peak loading level, as given in Eq. (55) [50]. The enhancement is determined by comparing the obtained index value with the corresponding value in the uncompensated system.

$$TI_{VD} = \sum_{i=1}^{n} (1 - V_i)^2, \forall i \in n, s = Pk \tag{55}$$

Enhancement of the Loading Capacity (TI_{LC})

The loading capacity of the branch currents is formulated by determining the maximum branch current, as given in Eq. (56), where $I_{max,br}$ is the maximum branch current allowed to flow.

$$TI_{LC} = \max \left(\frac{I_{br}}{I_{max,br}} \right), \forall br \in N_{br}, s = Pk \tag{56}$$

Voltage Stability Improvement (TI_{VS})

The VS enhancement is formulated by determining the minimum *VSI* calculated at all buses [31], as given in Eq. (57) and comparing its value with the uncompensated case.

$$TI_{VS} = \min [VSI_{bus}] = V_i^4 - 4(PX - QR)^2 - 4V_i^2 (PR + QX), \forall i \in n \tag{57}$$

7.2   Economic Indices

DGs Costs (EI_{DG})

EI_{DG} (\$/year) is formulated as given in (58), where R_{DG} represents DGs' operation and maintenance costs. RF_{DG} denotes the capital recovery factors of DGs used to convert the present value cost to annualized cost. R_{DG} is set to \$5/W [33].

$$EI_{DG} = R_{DG} \times RF_{DG} \sum_{g=1}^{N_{DG}} P_{DG}(g) \tag{58}$$

SCBs Costs (EI$_{SCB}$)

EI$_{SCB}$ (\$/year) is formulated as given in (59), where R_{SCB} represents SCBs' operation costs, CSCB means SCBs' investment costs, and RF$_{SCB}$ denotes SCBs' capital recovery factors. R_{SCB} and C_{SCB} are set to 30 \$/kvar and \$1000, respectively [33].

$$EI_{SCB} = R_{SCB} \left[C_{SCB} + RF_{SCB} \sum_{c=1}^{N_{SCB}} Q_{SCB}(c) \right] \tag{59}$$

VRs Costs (EI$_{VR}$)

EI$_{VR}$ (\$/year) is formulated in (60), where RF$_{VR}$ represents VRs' investment and operation costs. RF$_{SCB}$ denotes the capital recovery factors of SCBs. R_0 is the VR's cost (\$) that relies on the current rating of the VR (I_{VR}). For instance, R_0 equals \$38,000 for 100 A, \$44,800 for 150 A, \$50,600 for 200 A, \$58,100 for 250 A, \$64,700 for 300 A, \$70,300 for 350 A, and \$77,900 for 400 A [33].

$$EI_{VR} = RF_{VR} \times R_0 (I_{VR}) \tag{60}$$

A generalized expression of the recovery factors of the different compensators (RFc) is expressed in (61), where I is the interest rate (7%) and Y is the operation number of years of the compensator – 20 years for the DGs, 10 years for the SCBs, and 15 years for the VRs.

$$RF_c = \frac{I(1+I)^Y}{(1+I)^Y - 1}, \forall \ c = \{DG, SCB, VR\} \tag{61}$$

Returned Funds from Savings (EI$_{SAV}$)

Finally, the returned funds or savings are expressed in Eq. (62) as the difference between benefits and costs.

$$EI_{SAV} = [TI_P + TI_S] - [EI_{DG} + EI_{SCB} + EI_{VR}] \tag{62}$$

EI$_{SAV}$ is calculated while considering the three Lig, Sh, and Pk levels.

8 System Studied

Figure 14 explores the studied radial distribution system in Menoufia, Egypt. It comprises 37 buses supplied from 11 kV–50 Hz substation to feed 31 loads. P_d is 4.8019 MW, and the Q_d is 2.9759 MVAr. The base MVA and voltage are set to
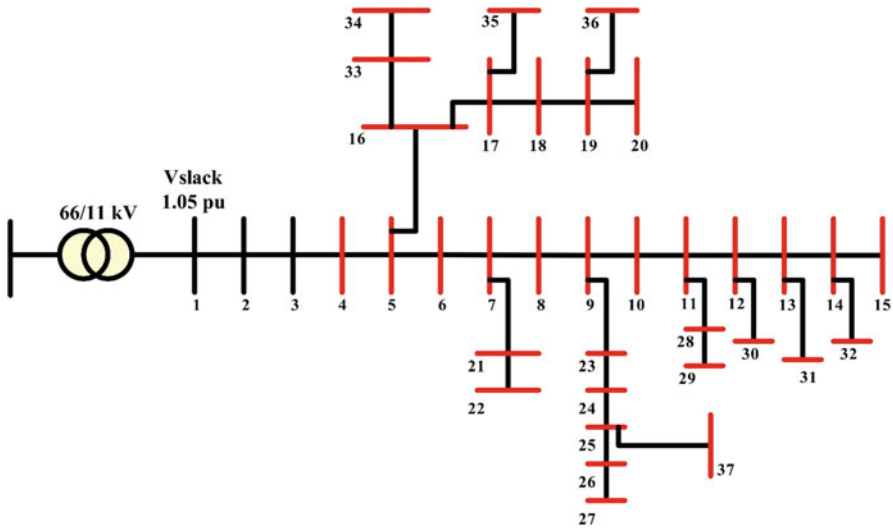
Fig. 14 Line diagram of the 37-bus radial distribution system studied

Table 3 Line data of the 37-bus system

br	From i	To j	I_{max} (A)	R (Ω)	X (Ω)	br	From i	To j	I_{max} (A)	R (Ω)	X (Ω)
1	1	2	788.00	0.0349	0.0493	19	19	20	183.70	0.4004	0.1540
2	2	3	788.00	0.1862	0.2629	20	7	21	183.70	0.8425	0.3240
3	3	4	788.00	1.2891	1.8201	21	21	22	183.70	0.2086	0.0802
4	4	5	788.00	1.1640	1.6434	22	9	23	183.70	1.4015	0.5389
5	5	6	367.50	0.0776	0.1096	23	23	24	183.70	0.5005	0.1925
6	6	7	367.50	0.0466	0.0657	24	24	25	183.70	0.5798	0.2230
7	7	8	367.50	0.0388	0.0548	25	25	26	183.70	0.6006	0.2310
8	8	9	367.50	0.1263	0.1534	26	26	27	183.70	0.4004	0.1540
9	9	10	367.50	0.1240	0.0893	27	11	28	183.70	0.9009	0.3465
10	10	11	367.50	0.2066	0.1489	28	28	29	183.70	1.1011	0.4235
11	11	12	367.50	0.1240	0.0893	29	12	30	183.70	0.2066	0.1489
12	12	13	367.50	0.1269	0.0914	30	13	31	183.70	0.2252	0.0866
13	13	14	367.50	0.0901	0.0649	31	14	32	183.70	0.4371	0.1681
14	14	15	367.50	0.2587	0.1864	32	16	33	183.70	0.1668	0.0642
15	5	16	183.70	0.7007	0.2695	33	33	34	183.70	0.4755	0.1829
16	16	17	183.70	0.2002	0.0770	34	17	35	183.70	0.6006	0.2310
17	17	18	183.70	0.7007	0.2695	35	19	36	183.70	1.1011	0.4235
18	18	19	183.70	0.9009	0.3465	36	25	37	183.70	0.5005	0.1925

1 MVA and 11 kV, respectively. The complete system data are presented in Tables 3 and 4 [33]. All the buses given in red indicate a violation of the voltage limits (less than 0.9 pu), and this shows that the investigated electrical system is a deteriorated system that suffers from a low voltage profile, such that the minimum voltage is

Table 4 Load data of the 37-bus system at the three different loading levels

	Pk		Sh		Lig	
Bus i	P_i (kW)	Q_i (kVAr)	P_i (kW)	Q_i (kVAr)	P_i (kW)	Q_i (kVAr)
1	0	0	0	0	0	0
2	0	0	0	0	0	0
3	21.2003	13.1388	16.9602	10.511	12.7202	7.88328
4	10.6002	6.5694	8.48016	5.25552	6.36012	3.94164
5	117.7795	72.9932	94.2236	58.3946	70.6677	43.7959
6	255.5814	158.3951	204.465	126.716	153.349	95.0371
7	127.2018	78.8326	101.761	63.0661	76.3211	47.2996
8	0	0	0	0	0	0
9	0	0	0	0	0	0
10	138.9798	86.1319	111.184	68.9055	83.3879	51.6791
11	181.3804	112.4095	145.104	89.9276	108.828	67.4457
12	152.5244	94.5261	122.02	75.6209	91.5146	56.7157
13	0	0	0	0	0	0
14	221.4254	137.2271	177.14	109.782	132.855	82.3363
15	241.4479	149.6360	193.158	119.709	144.869	89.7816
16	42.4006	26.2775	33.9205	21.022	25.4404	15.7665
17	144.8687	89.7816	115.895	71.8253	86.9212	53.869
18	26.5004	16.4235	21.2003	13.1388	15.9002	9.8541
19	41.8117	25.9126	33.4494	20.7301	25.087	15.5476
20	66.5454	41.2411	53.2363	32.9929	39.9272	24.7447
21	325.0713	201.4611	260.057	161.169	195.043	120.877
22	214.9475	133.2125	171.958	106.57	128.969	79.9275
23	113.0683	70.0734	90.4546	56.0587	67.841	42.044
24	121.9017	75.5479	97.5214	60.4383	73.141	45.3287
25	175.4914	108.7598	140.393	87.0078	105.295	65.2559
26	94.2236	58.3945	75.3789	46.7156	56.5342	35.0367
27	118.3684	73.3581	94.6947	58.6865	71.021	44.0149
28	299.1598	185.4026	239.328	148.322	179.496	111.242
29	215.5364	133.5775	172.429	106.862	129.322	80.1465
30	0	0	0	0	0	0
31	241.4479	149.6360	193.158	119.709	144.869	89.7816
32	267.9483	166.0594	214.359	132.848	160.769	99.6356
33	276.1928	171.1689	220.954	136.935	165.716	102.701
34	106.0015	65.6938	84.8012	52.555	63.6009	39.4163
35	256.7592	159.1251	205.407	127.3	154.056	95.4751
36	10.6002	6.5694	8.48016	5.25552	6.36012	3.94164
37	174.9025	108.3948	139.922	86.7158	104.942	65.0369
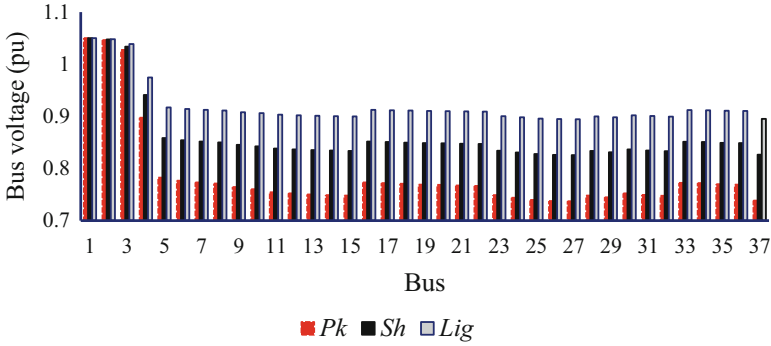
Fig. 15 Uncompensated voltage profile of the studied system at the three loading levels
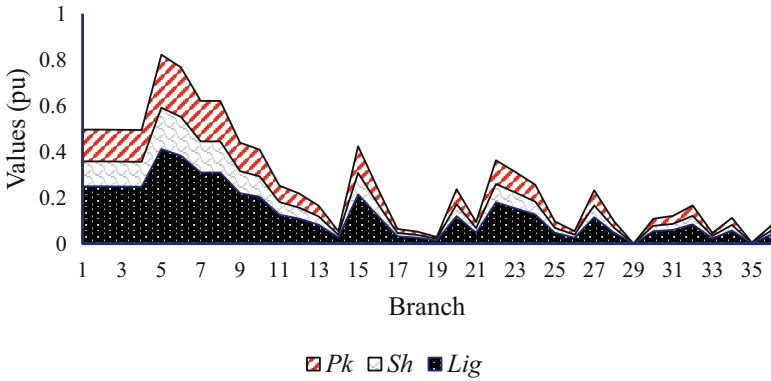
Fig. 16 Loading capacity of the branches of the studied system at the three loading levels

measured at bus #27 and equals 0.7371 pu. Also, the 37-bus system suffers from very high-apparent power losses (higher than 1 MW for active power losses and 1.8 MVAr for reactive power losses in the period of the maximum demand). The slack bus voltage is set to 1.05 pu.

The 37-bus system has three different loading levels, Lig, Sh, and Pk, each of which continues for 2920 hours (i.e., 8760/3 hours) as mentioned before.

The voltage magnitudes of the 37 buses are explored in Fig. 15 at the three loading levels before compensation. Figure 16 explores the loading capacity of the branches at the three loading levels. Noticeably, the system undergoes poor voltage regulation, highly active and reactive power losses, and expected current problems, principally at the *Pk* level. The insufficient voltage is caused because the system includes long branches (around 13 km for branches 3–4 and 4–5). These branches will be considered candidate locations to allocate VRs.

The technical QoP indices used are presented in Table 5 for the uncompensated 37-bus system in which P_{loss} (kW), Q_{loss} (kVAr), S_{grid} (MVA), minimum (V_{min})

Table 5 Results of the uncompensated 37-bus studied system

QoP metric		Loading levels					
		Lig		Sh		Pk	
P_{loss} (kW)		343.1828		707.4094		1361.7	
Q_{loss} (kVAr)		463.8976		956.0957		1839.9	
S_{grid} (MVA)		3.9312		5.6414		7.8213	
V_{min} (pu)	Bus	0.8946	27	0.8259	27	0.7371	27
V_{max} (pu)	Bus	1.05	1	1.05	1	1.05	1
Loading capacity (%)		41.12		59.10		82.15	
Minimum *VSI* (pu)		0.6406		0.4652		0.2952	

voltage magnitude (pu) and its bus number, loading capacity of the branches in percentage, and the minimum *VSI* are calculated at the three loading levels.

9   Results and Discussions

The decision variables of the problem formulated are the DGs and SCBs – locations and sizes and the tapping of the VR. One to three DGs, $1 \leq N_{\text{DG}} \leq 3$, can connect to the system. Also, one to eight SCBs can connect to the system ($N_{\text{SCB}} \leq 8$). The probable locations of DGs and SCBs are specified as integer variables between 2 and 37 (bus #2 to bus #37). DG sizes are expressed as continuous variables that range between 0 kW and 5 MW. SCBs sizes are considered as discrete variables ranging between 0 and 1200 kVAr. SCBs size is deemed to be in steps of 150 kVAr. The maximum number of SCBs and DGs to be located is 12 (8 SCBs and 3 DGs, in addition to one VR with two variables (location and size)). The VR cost and the current capacity are taken from [29].

Six cases are investigated – Case #1: DGs allocation, Case #2: SCBs allocation, Case #3: DGs/SCBs coordination, Case #4: DGs/VRs coordination, Case #5: SCBs/VRs coordination, and Case #6: DGs/SCBs/VRs coordination. The results of the six cases are reported in the following subsections, and a comparison between them is given. It should be noted that the number of populations is 30, and 2000 iterations are set. The sizes, locations, and tap settings of the VRs obtained in the various cases are tabulated in Table 6. Table 7 shows the objective function values obtained and the time needed to reach them in all cases investigated.

It is evident that the lowest objective function was achieved when f_6 – DGs/SCBs/VRs –was used (17.208 MW), followed by f_3 – DGs/SCBs – (51.279 MW). This means that coordinating the compensators is necessary to achieve good results. On the other side, the worst objective function was performed when f_2 – SCBs – was used (475.472 MW). However, f_6 needs considerable computation time to be executed (33.78 minutes) compared with the other objective functions.

Tables 8, 9, and 10 show the compensated bus voltage values at the different cases investigated in the three scenarios (Lig, Sh, Pk), respectively. As is obvious,

Table 6 Sizes, locations and tap settings of the VRs obtained in the various cases

Case #1	DGs	Size (kW)	1316.6872, 2084.5915, 709.5161
		Location (bus)	13,5, 25
Case #2	SCBs	Size (kVAr)	750, 600, 1200, 150, 900, 150, 150
		Location (bus)	26, 10, 8, 15, 5, 11, 2
Case #3	DGs	Size (kW)	100, 3571.50, 100
		Location (bus)	25, 9, 13
	SCBs	Size (kVAr)	300, 150, 750, 150, 750, 450, 600
		Location (bus)	2, 20, 5, 29, 23, 14, 2
Case #4	DGs	Size (kW)	1859.204, 1121.695, 2212.0772
		Location (bus)	2, 12, 7
	VRs	Location (bus)	Between buses 3 and 4
		Tapping (Lig, Sh, Pk)	−2, 2, 13
Case #5	SCBs	Size (kVAr)	450, 900, 450, 750, 300, 300, 300
		Location (bus)	3, 12, 2, 6, 25, 2, 2
	VRs	Location (bus)	Between buses 3 and 4
		Tapping (Lig, Sh, Pk)	0, 10, 16
Case #6	DGs	Size (kW)	478.3795, 2182.7499, 730.6741
		Location (bus)	18, 11, 8
	SCBs	Size (kVAr)	300, 450, 450, 300, 300, 450, 300
		Location (bus)	14, 2, 7, 11, 15, 8, 17
	VRs	Location (bus)	Between buses 3 and 4
		Tapping (Lig, Sh, Pk)	−9, −7, −4

Table 7 Objective function values and the time needed to attain them

Cases	#1	#2	#3	#4	#5	#6
f (MW)	187.680	475.472	51.279	91.342	203.636	17.208
Time (s)	232.043	313.000	260.030	11,948.911	19,465.457	2,026.202

the voltage profiles have been enhanced at the three loading scenarios and thereby meet the permissible limits (among all cases, the lowest voltage value is 0.9 pu in the peak loading).

Tables 11, 12, and 13 show the compensated branch current values at the different cases investigated in the three scenarios, respectively. Compared with the I_{max} values given in Table 3, the current values have been reduced at the three loading scenarios and are lower than the maximum branch current values.

Table 14 shows the technical performance metrics calculated in all cases under study. Regarding the active power loss reduction (kW), the best reduction value obtained was in Case #3 as 2258.462 kW in DGs/SCBs coordination, followed by 2251.906 in DGs/SCBs/VRs coordination. This means that minimizing the power loss as an objective function is not the best choice, as maximizing the benefits can achieve better results.

Table 8 Bus voltage values at the different cases investigated, Lig

Cases Bus	#1	#2	#3	#4	#5	#6	Cases Bus	#1	#2	#3	#4	#5	#6
1	1.05	1.05	1.05	1.05	1.05	1.05	20	1.01	1.04	1.09	0.98	0.98	1.02
2	1.05	1.05	1.05	1.05	1.05	1.05	21	1.01	1.05	1.09	0.99	0.98	1.01
3	1.05	1.05	1.05	1.05	1.05	1.05	22	1.01	1.05	1.09	0.99	0.98	1.01
4	1.03	1.05	1.08	1.01	1.01	1.01	23	1.02	1.05	1.10	0.98	0.98	1.01
5	1.02	1.05	1.09	0.99	0.99	1.02	24	1.02	1.05	1.10	0.98	0.97	1.01
6	1.02	1.05	1.10	0.99	0.98	1.02	25	1.02	1.04	1.10	0.98	0.97	1.01
7	1.02	1.05	1.10	0.99	0.98	1.02	26	1.02	1.05	1.09	0.98	0.97	1.01
8	1.02	1.05	1.10	0.99	0.98	1.02	27	1.02	1.05	1.09	0.97	0.97	1.01
9	1.02	1.05	1.10	0.99	0.98	1.02	28	1.01	1.04	1.09	0.98	0.98	1.02
10	1.02	1.05	1.10	0.99	0.98	1.02	29	1.01	1.04	1.09	0.98	0.97	1.02
11	1.02	1.05	1.10	0.99	0.98	1.02	30	1.02	1.05	1.10	0.99	0.98	1.02
12	1.02	1.05	1.10	0.99	0.98	1.02	31	1.02	1.04	1.10	0.98	0.98	1.02
13	1.02	1.04	1.10	0.98	0.98	1.02	32	1.01	1.04	1.10	0.98	0.98	1.02
14	1.02	1.04	1.10	0.98	0.98	1.02	33	1.01	1.04	1.09	0.99	0.98	1.02
15	1.01	1.04	1.10	0.98	0.98	1.02	34	1.01	1.04	1.09	0.99	0.98	1.01
16	1.02	1.05	1.09	0.99	0.98	1.02	35	1.01	1.04	1.09	0.98	0.98	1.01
17	1.01	1.04	1.09	0.99	0.98	1.02	36	1.01	1.04	1.09	0.98	0.98	1.02
18	1.01	1.04	1.09	0.98	0.98	1.02	37	1.02	1.04	1.09	0.98	0.97	1.01
19	1.01	1.04	1.09	0.98	0.98	1.02							

Table 9 Bus voltage values at the different cases investigated, Sh

Cases Bus	#1	#2	#3	#4	#5	#6	Cases Bus	#1	#2	#3	#4	#5	#6
1	1.05	1.05	1.05	1.05	1.05	1.05	20	0.97	0.98	1.05	0.94	1.00	0.99
2	1.05	1.05	1.05	1.05	1.05	1.05	21	0.97	0.99	1.05	0.94	1.00	0.98
3	1.04	1.04	1.05	1.04	1.04	1.05	22	0.97	0.99	1.05	0.94	1.00	0.98
4	1.01	1.01	1.05	0.99	1.05	1.00	23	0.97	0.98	1.05	0.93	0.99	0.98
5	0.98	0.99	1.05	0.95	1.01	0.99	24	0.97	0.98	1.05	0.93	0.99	0.97
6	0.98	0.99	1.05	0.95	1.01	0.99	25	0.97	0.98	1.05	0.92	0.99	0.97
7	0.97	0.99	1.05	0.94	1.01	0.99	26	0.97	0.98	1.04	0.92	0.99	0.97
8	0.97	0.99	1.05	0.94	1.01	0.99	27	0.97	0.98	1.04	0.92	0.99	0.97
9	0.97	0.99	1.05	0.94	1.00	0.99	28	0.97	0.98	1.05	0.93	0.99	0.98
10	0.97	0.99	1.05	0.94	1.00	0.99	29	0.96	0.98	1.05	0.93	0.99	0.98
11	0.97	0.98	1.05	0.94	1.00	0.99	30	0.97	0.98	1.05	0.94	1.00	0.99
12	0.97	0.98	1.05	0.94	1.00	0.99	31	0.97	0.98	1.05	0.94	1.00	0.99
13	0.97	0.98	1.05	0.94	1.00	0.99	32	0.97	0.98	1.05	0.93	1.00	0.98
14	0.97	0.98	1.05	0.94	1.00	0.99	33	0.97	0.99	1.05	0.94	1.00	0.98
15	0.97	0.98	1.05	0.93	1.00	0.99	34	0.97	0.99	1.05	0.94	1.00	0.98
16	0.97	0.99	1.05	0.94	1.00	0.98	35	0.97	0.98	1.04	0.94	1.00	0.98
17	0.97	0.99	1.05	0.94	1.00	0.98	36	0.97	0.98	1.04	0.94	1.00	0.99
18	0.97	0.99	1.05	0.94	1.00	0.99	37	0.97	0.98	1.04	0.92	0.99	0.97
19	0.97	0.98	1.05	0.94	1.00	0.99							

Table 10 Bus voltage values at the different cases investigated, Pk

Cases							Cases						
Bus	#1	#2	#3	#4	#5	#6	Bus	#1	#2	#3	#4	#5	#6
1	1.05	1.05	1.05	1.05	1.05	1.05	20	0.92	0.91	1.00	0.99	0.99	0.96
2	1.05	1.05	1.05	1.05	1.05	1.05	21	0.92	0.92	1.00	1.00	0.99	0.95
3	1.04	1.04	1.05	1.04	1.04	1.04	22	0.92	0.91	1.00	1.00	0.99	0.95
4	0.98	0.98	1.02	1.06	1.06	0.99	23	0.92	0.91	1.00	0.98	0.98	0.94
5	0.93	0.92	1.00	1.00	1.00	0.96	24	0.92	0.90	0.99	0.98	0.98	0.94
6	0.93	0.92	1.00	1.00	1.00	0.96	25	0.92	0.90	0.99	0.98	0.97	0.94
7	0.93	0.92	1.00	1.00	0.99	0.96	26	0.92	0.90	0.99	0.98	0.97	0.93
8	0.93	0.92	1.00	1.00	0.99	0.96	27	0.92	0.90	0.99	0.97	0.97	0.93
9	0.92	0.92	1.00	1.00	0.99	0.96	28	0.91	0.90	0.99	0.99	0.98	0.95
10	0.92	0.91	1.00	0.99	0.99	0.96	29	0.91	0.90	0.99	0.98	0.98	0.95
11	0.92	0.91	1.00	0.99	0.98	0.96	30	0.92	0.91	1.00	0.99	0.98	0.95
12	0.92	0.91	1.00	0.99	0.98	0.95	31	0.92	0.91	1.00	0.99	0.98	0.95
13	0.92	0.91	1.00	0.99	0.98	0.95	32	0.92	0.90	0.99	0.99	0.98	0.95
14	0.92	0.90	1.00	0.99	0.98	0.95	33	0.92	0.92	1.00	1.00	0.99	0.95
15	0.92	0.90	0.99	0.99	0.98	0.95	34	0.92	0.92	1.00	1.00	0.99	0.95
16	0.92	0.92	1.00	1.00	0.99	0.96	35	0.92	0.91	1.00	0.99	0.99	0.95
17	0.92	0.92	1.00	1.00	0.99	0.96	36	0.92	0.91	1.00	0.99	0.99	0.96
18	0.92	0.91	1.00	0.99	0.99	0.96	37	0.92	0.90	0.99	0.98	0.97	0.93
19	0.92	0.91	1.00	0.99	0.99	0.96							

Regarding the reactive power loss reduction (kVAr), the best reduction value obtained was in Case #3 as 3112.182 kVAr in DGs/SCBs coordination, followed by 3098.964 kVAr in DGs/SCBs/VRs coordination. However, in terms of the capacity release in MVA, the best value obtained was in Case #6 as 14.233 MVA in DGs/SCBs/VRs coordination, followed by 13.163 MVA in DGs/SCBs coordination.

At $s = $ Pk, the *VSI* values are improved when any of the six cases are applied. However, it is also clear that a significant improvement is obtained when both DGs/SCBs and DGs/VRs are connected to the system. So, Cases #3 and #4 have had a better impact on VS than others. Besides, at $s = $ Pk, the best TI_{VD} and TI_{LC} were obtained while employing Case #3.

Table 15 shows the economic performance metrics calculated in all cases under study. The best EI_{SAV} was obtained in Case #3 (10.4488 million $/year), while a no saving case was observed in Case #4 (-0.6989 million $/year). It was expected that the economic performance metrics would be low in cases including VRs because of their added capital costs.

Finally, Table 16 explores the active power loss values calculated on heavy demands using different algorithms in the literature, such as particle swarm, grey wolf, sine cosine, and the proposed whale algorithm. The results validate the effectiveness and the superiority of the proposed algorithm in solving the formulated problem.

Table 11 Branch currents values at the different cases investigated, Lig

Cases Branch	#1	#2	#3	#4	#5	#6
1	111.70	190.50	101.51	146.14	170.80	49.86
2	111.70	186.10	59.93	96.88	155.39	30.70
3	111.68	185.77	60.65	96.62	154.22	31.44
4	111.69	185.62	61.00	97.70	153.88	33.60
5	71.63	141.72	74.98	93.86	121.56	43.88
6	66.07	138.85	83.02	95.52	110.83	53.18
7	56.41	133.98	104.49	61.91	89.33	67.12
8	56.41	92.16	104.49	61.91	89.33	27.06
9	38.44	60.47	51.56	39.00	63.64	52.67
10	36.91	57.69	47.61	36.16	59.59	57.44
11	39.57	36.27	28.16	32.57	43.34	36.31
12	42.23	30.98	24.69	36.60	36.90	32.93
13	26.68	22.72	24.63	27.52	27.74	28.97
14	8.81	8.17	8.17	9.09	9.17	13.67
15	35.50	34.47	29.45	36.54	36.75	6.10
16	20.00	19.42	15.87	20.58	20.70	9.44
17	5.32	5.17	7.31	5.48	5.51	20.36
18	4.35	4.22	7.31	4.48	4.50	4.33

Cases Branch	#1	#2	#3	#4	#5	#6
19	2.43	2.36	7.63	2.51	2.52	2.42
20	19.73	19.11	18.30	20.28	20.41	19.72
21	7.85	7.61	7.29	8.07	8.13	7.85
22	19.37	35.71	34.23	30.28	25.86	29.32
23	20.21	35.15	19.27	26.00	22.25	25.18
24	21.96	35.07	15.19	21.39	18.68	20.71
25	7.73	37.73	7.20	8.08	8.11	7.82
26	4.31	4.20	4.01	4.50	4.52	4.36
27	18.85	18.29	14.83	19.42	19.57	18.72
28	7.90	7.66	7.83	8.14	8.20	7.85
29	0.00	0.00	0.00	0.00	0.00	0.00
30	8.81	8.57	8.16	9.09	9.16	8.76
31	9.78	9.51	9.06	10.09	10.18	9.73
32	13.96	13.55	12.99	14.37	14.45	13.95
33	3.87	3.76	3.60	3.99	4.01	3.87
34	9.39	9.11	8.73	9.66	9.72	9.37
35	0.39	0.38	0.36	0.40	0.40	0.39
36	6.36	6.21	5.92	6.64	6.67	6.43

Table 12 Branch currents values at the different cases investigated, Sh

Cases Branch	#1	#2	#3	#4	#5	#6
1	129.43	217.56	53.91	142.81	214.50	24.84
2	129.43	216.03	6.30	134.53	212.98	29.83
3	128.94	215.29	6.07	133.81	215.92	28.84
4	128.71	214.93	6.01	131.77	201.96	29.58
5	110.86	165.19	43.92	101.40	155.07	5.12
6	100.02	157.11	51.69	97.58	146.95	8.56
7	74.86	139.34	77.35	95.72	116.86	36.89
8	74.86	118.95	77.35	95.72	116.86	26.67
9	54.51	84.05	75.19	58.43	82.75	32.86
10	49.62	84.62	69.08	52.63	76.82	38.38
11	37.69	53.00	40.19	32.71	50.63	47.96
12	39.12	45.40	33.97	49.95	48.24	41.79
13	37.28	33.41	30.03	37.55	36.26	33.29
14	12.32	10.42	11.39	12.41	11.98	13.76
15	49.44	48.71	42.18	49.68	47.89	19.01
16	27.85	27.44	22.65	27.99	26.98	2.33
17	7.41	7.30	7.44	7.45	7.18	19.64
18	6.06	5.97	7.11	6.09	5.87	5.96

Cases Branch	#1	#2	#3	#4	#5	#6
19	3.39	3.34	7.09	3.41	3.28	3.34
20	27.49	27.03	25.45	27.59	26.62	27.15
21	10.94	10.76	10.13	10.98	10.60	10.81
22	21.75	38.49	34.55	41.39	34.25	40.58
23	20.33	35.83	28.22	35.56	29.15	34.85
24	20.57	33.83	22.50	29.25	23.90	28.67
25	10.82	34.16	10.06	11.05	10.62	10.83
26	6.03	5.97	5.60	6.15	5.91	6.03
27	26.36	25.97	21.16	26.51	25.58	25.87
28	11.05	10.89	9.12	11.11	10.72	10.84
29	0.00	0.00	0.00	0.00	0.00	0.00
30	12.31	12.16	11.38	12.40	11.97	12.10
31	13.68	13.51	12.64	13.77	13.30	13.44
32	19.43	19.14	18.05	19.53	18.82	19.20
33	5.39	5.31	5.01	5.42	5.22	5.33
34	13.08	12.88	12.14	13.14	12.66	12.90
35	0.54	0.53	0.50	0.54	0.52	0.53
36	8.90	8.83	8.27	9.09	8.73	8.91

Table 13 Branch currents values at the different cases investigated, Pk

Cases Branch	#1	#2	#3	#4	#5	#6
1	174.54	276.32	56.07	169.72	274.99	83.30
2	174.54	277.32	68.36	191.89	284.67	96.17
3	173.61	276.17	67.11	190.80	290.71	94.93
4	173.13	275.59	66.48	174.77	261.04	96.64
5	161.33	213.02	50.33	122.67	197.93	56.51
6	145.71	198.79	45.08	112.88	190.76	40.23
7	106.72	164.10	55.42	126.36	151.09	27.89
8	106.72	161.63	55.42	126.36	151.09	59.58
9	78.91	116.88	103.45	78.52	106.67	25.01
10	71.00	117.41	95.13	70.68	98.64	26.04
11	41.39	73.27	55.68	37.05	60.94	62.59
12	39.70	62.93	46.79	60.81	61.31	53.72
13	49.27	46.56	38.58	45.72	46.09	40.62
14	16.28	14.10	14.99	15.10	15.23	14.92
15	65.05	65.57	56.51	60.29	60.62	32.68
16	36.66	36.95	30.55	33.97	34.16	5.29
17	9.76	9.83	8.27	9.04	9.09	18.91
18	7.98	8.04	7.41	7.39	7.44	7.69

Cases Branch	#1	#2	#3	#4	#5	#6
19	4.46	4.50	6.66	4.14	4.16	4.30
20	36.20	36.43	33.40	33.50	33.72	35.02
21	14.41	14.51	13.30	13.34	13.43	13.94
22	28.78	47.05	39.24	50.42	44.52	52.61
23	24.34	41.41	38.29	43.32	37.75	45.21
24	21.64	36.20	30.74	35.64	30.62	37.19
25	14.33	30.43	13.27	13.47	13.52	14.06
26	7.98	8.12	7.39	7.50	7.53	7.83
27	34.86	35.21	28.68	32.27	32.52	33.48
28	14.62	14.77	11.43	13.53	13.64	14.04
29	0.00	0.00	0.00	0.00	0.00	0.00
30	16.26	16.47	14.98	15.09	15.21	15.66
31	18.08	18.31	16.65	16.77	16.91	17.40
32	25.56	25.76	23.67	23.69	23.82	24.73
33	7.09	7.15	6.57	6.57	6.61	6.86
34	17.21	17.35	15.93	15.95	16.04	16.63
35	0.71	0.72	0.66	0.66	0.66	0.69
36	11.78	12.00	10.91	11.07	11.12	11.55

Table 14 Technical performance metrics calculated in all cases under study

Cases	Scenario	Base case	#1	#2	#3	#4	#5	#6
P_{loss} (kW)	Lig	343.2	115.2296	311.4027	51.5445	96.5471	215.955	23.7434
	Sh	707.4	159.2406	421.3609	26.5525	177.2899	394.6647	27.7864
	Pk	1361.7	288.5721	693.6539	75.741	96.5471	686.5978	108.8639
Q_{loss} (kVAr)	Lig	463.9	151.3254	418.1321	59.0815	122.0755	289.9842	21.013
	Sh	956.1	206.3696	563.7286	16.4286	223.6043	531.9385	19.21
	Pk	1839.9	375.7626	928.5421	72.208	418.4663	928.0445	120.7133
S_{grid} (MVA)	Lig	3.9312	2.2345	3.811	2.0308	2.9235	3.417	0.9975
	Sh	5.6414	2.5893	4.3524	1.0784	2.8569	4.291	0.497
	Pk	7.8213	3.4918	5.5278	1.1217	3.3953	5.5011	1.6664
$P_{loss,tot}$ (kW)		2412.3	563.0423	1426.418	153.838	370.3841	1297.218	160.3937
$Q_{loss,tot}$ (kVAr)		3259.9	733.4576	1910.403	147.7181	764.1461	1749.967	160.9363
$S_{grid,tot}$ (MVA)		17.3939	8.3156	13.6912	4.2309	9.1757	13.2091	3.1609
TI_{VS}	Lig	0.6406	1	1	1	0.8561	0.7828	0.947
	Sh	0.4652	0.861	0.9141	1	0.7694	0.8894	0.8573
	Pk	0.2952	0.6859	0.6563	0.9564	0.87	0.7762	0.7601
Active power loss reduction (kW)			1849.258	985.8825	2258.462	2041.916	1115.083	2251.906
Reactive power loss reduction (kVAr)			2526.442	1349.497	3112.182	2495.754	1509.933	3098.964
Capacity release (MVA)			9.0783	3.7027	13.163	8.2182	4.1848	14.233
TI_{VD} ($s = Pk$)		1.9425	0.1739	0.2162	0.0085	0.0149	0.0201	0.0881
TI_{LC} ($s = Pk$)		0.8218	0.439	0.5796	0.1976	0.3438	0.5386	0.2864

Table 15 Economic performance metrics calculated in all cases under study

Cases						
Costs	#1	#2	#3	#4	#5	#6
EI$_{DG}$ (million $/year)	1.9401	0	1.7800	2.4509	0	1.6008
EI$_{SCB}$ (million $/year)	0	0.0168	0.0136	0	0.0149	0.0110
EI$_{VR}$ (million $/year)	0	0	0	0.0056	0.0071	0.0042
Benefits (TI$_P$+ TI$_S$) (million $/year)	11.4550	10.3620	12.2424	1.7576	0.9285	2.8882
EI$_{SAV}$ (million $/year)	9.5149	10.3452	10.4488	−0.6989	0.9065	1.2721

Table 16 Active power loss calculated on heavy demands using different algorithms in the literature

$P_{loss, peak}$ (kW)	Algorithm	Ref.	Compensator		
			DGs	SCBs	VRs
288.5721	Whale	Proposed	✓	×	×
693.6539			×	✓	×
75.741			✓	✓	×
96.5471			✓	×	✓
686.5978			×	✓	✓
108.8639			✓	✓	✓
740.32	Particle swarm	[49]	×	✓	×
302.74			✓	×	×
1122.15			×	×	✓
438.29			✓	✓	✓
134.4	Grey wolf	[33]	✓	✓	×
341.00			✓	×	×
580.3			×	✓	×
413.4			✓	×	✓
340.9671	Sine cosine	Proposed	✓	×	×
699.4165			×	✓	×
216.6044			✓	✓	×

10 Conclusions

Integration of active and reactive power compensators into power networks should be arranged not to pose problems in these systems but to enjoy the benefits and avoid the issues. To do this, finding the optimal location and size of these compensators in a system is necessary. Economically speaking, the rising project investment may result if uneconomic facilities or expensive technologies are used to reduce electric losses significantly. Also, high investment expenses limit renewables-based technologies to generate electricity, but these costs decline over days. Therefore, economic considerations related to the installed network equipment should be considered. In this regard, the well-known WOA is applied in this work to allocate DGs, SCBs, and VRs in a realistic 37-bus distribution system to minimize power

losses while conforming with several linear and nonlinear constraints. A cost-benefit analysis of the optimization problem is presented in terms of – investment and running costs of the compensators used; saving gained from the power loss reduction and benefits from decreasing the power to be purchased from the grid; reducing voltage deviations and overloading; and enhancing VS. Three loading scenarios are addressed in this work – Lig, Sh, and Pk levels of load demand. The numerical findings obtained show a noteworthy techno-economic improvement of the QoP performance level of the RDS and approve the efficiency and economic benefits of the proposed solutions compared to other solutions in the literature.

The main remarks that have been concluded during this research work are that the proposed coordination of DGs/SCBs and DGs/SCBs/VRs can effectively enhance the QoP levels to comply with the Egyptian practice code limits. They showed efficient savings results, particularly when considering techno-economic aspects together. They showed acceptable steady-state voltage profiles that comply with the standard limits and considerable power loss reduction in addition to the released capacity of the power distribution transformer. The coordination of active and reactive power conditioners showed that the best performance metrics values were obtained using the optimal coordination of DGs/SCBs and DGs/SCBs/VRs. However, it was also clear that a significant improvement was obtained when DGs/SCBs were connected to the system, leading to better impacts. The benefits of adding VRs will advance if higher loading levels are investigated but on the economic advantages side.

Finally, the results confirm that WOA is a powerful optimization tool in convergence and exploration-exploitation balance. Also, it is well applicable to solve more complex engineering problems. However, it should be noted that no optimization algorithm can solve all problems, but one algorithm can solve a particular problem much more efficiently.

Future works will address combining the investigated objective functions and formulating the problem as a multi-objective optimization problem under uncertain conditions and parameters variations. Also, the allocation of fault current limiters and battery energy storage technologies shall investigate their impacts on the system's performance while considering the potential load growth/higher loading levels. Finally, recent metaheuristic optimization techniques can solve the optimization problem with more practical probabilistic considerations.

References

1. Bansal R (2017) Handbook of distributed generation. Springer International Publishing, Cham
2. Masoum MAS, Fuchs EF (2015) Power quality in power systems and electrical machines. Elsevier Academic Press, Cambridge, MA
3. Diaaeldin I, Abdel Aleem S, El-Rafei A, Abdelaziz A, Zobaa AF (2019) Optimal network reconfiguration in active distribution networks with soft open points and distributed generation. Energies 12(21):4172. https://doi.org/10.3390/en12214172
4. El-Khattam W, Salama MMA (2004) Distributed generation technologies, definitions and benefits. Electr Power Syst Res 71(2):119–128. https://doi.org/10.1016/j.epsr.2004.01.006

5. Diaaeldin IM, Abdel Aleem SHE, El-Rafei A, Abdelaziz AY, Zobaa AF (2020) Hosting capacity maximization based on optimal reconfiguration of distribution networks with optimized soft open point operation. In: Hosting capacity for smart power grids. Springer, Cham, pp 179–193.

6. Ismael SM, Abdel Aleem SHE, Abdelaziz AY, Zobaa AF (2019) State-of-the-art of hosting capacity in modern power systems with distributed generation. In: Renewable energy, vol 130. Elsevier, pp 1002–1020

7. Wei X, Qiu X, Xu J, Li X (2010) Reactive power optimization in smart grid with wind power generator. In: 2010 Asia-Pacific power and energy engineering conference, pp 1–4

8. Li L, Zeng X, Zhang P (2008) Wind farms reactive power optimization using genetic/tabu hybrid algorithm. In: 2008 international conference on intelligent computation technology and automation (ICICTA), vol 1, pp 1272–1276

9. Ardizzon G, Cavazzini G, Pavesi G (2014) A new generation of small hydro and pumped-hydro power plants: advances and future challenges. Renew Sust Energ Rev 31:746–761

10. Khatod DK, Pant V, Sharma J (2012) Evolutionary programming based optimal placement of renewable distributed generators. IEEE Trans Power Syst 28(2):683–695

11. Muttaqi KM, Le ADT, Negnevitsky M, Ledwich G (2014) An algebraic approach for determination of DG parameters to support voltage profiles in radial distribution networks. IEEE Trans Smart Grid 5(3):1351–1360

12. Ghanbari N, Mokhtari H, Bhattacharya S (2018) Optimal distributed generation allocation and sizing for minimizing losses and cost function. In: 2018 IEEE industry applications society annual meeting (IAS), pp 1–6

13. Ismael SM, Aleem SHEA, Abdelaziz AY (2018) Optimal sizing and placement of distributed generation in Egyptian radial distribution systems using crow search algorithm. In: Proceedings of 2018 International Conference on Innovative Trends in Computer Engineering, ITCE 2018, vol 2018-March, pp 332–337. https://doi.org/10.1109/ITCE.2018.8316646

14. Abdel-mawgoud H, Kamel S, Yu J, Jurado F (2019) Hybrid Salp swarm algorithm for integrating renewable distributed energy resources in distribution systems considering annual load growth. J King Saud Univ Inf Sci 34:1381. https://doi.org/10.1016/j.jksuci.2019.08.011

15. Kim T, Lee Y, Lee B, Song H, Kim T (2009) Optimal capacitor placement considering voltage stability margin based on improved PSO algorithm. In: 2009 15th international conference on intelligent system applications to power systems, ISAP '09, pp 1–5. https://doi.org/10.1109/ISAP.2009.5352890

16. Hijazi H, Coffrin C, Van Hentenryck P (2017) Convex quadratic relaxations for mixed-integer nonlinear programs in power systems. Math Program Comput 9(3):321–367. https://doi.org/10.1007/s12532-016-0112-z

17. Shaheen AM, El-Sehiemy RA, Farrag SM (2019) A reactive power planning procedure considering iterative identification of VAR candidate buses. Neural Comput Appl 31(3):653–674

18. Kannan SM, Renuga P, Kalyani S, Muthukumaran E (2011) Optimal capacitor placement and sizing using fuzzy-DE and fuzzy-MAPSO methods. Appl Soft Comput J 11(8):4997–5005. https://doi.org/10.1016/j.asoc.2011.05.058

19. Kumar A, Bhatia RS (2015) Optimal capacitor placement in radial distribution system. India Int Conf Power Electron IICPE 2015(4):630–637. https://doi.org/10.1109/IICPE.2014.7115763

20. Delfanti M, Granelli GP, Marannino P, Montagna M (2000) Optimal capacitor placement using deterministic and genetic algorithms. IEEE Trans Power Syst 15(3):1041–1046. https://doi.org/10.1109/59.871731

21. Park JY, Sohn JM, Park JK (2009) Optimal capacitor allocation in a distribution system considering operation costs. IEEE Trans Power Syst 24(1):462–468. https://doi.org/10.1109/TPWRS.2008.2009489

22. Ng HN, Salama MMA, Chikhani AY (2000) Classification of capacitor allocation techniques. IEEE Trans Power Deliv 15(1):387–392. https://doi.org/10.1109/61.847278

23. Diaaeldin I, Aleem SA, El-Rafei A, Abdelaziz A, Zobaa AF (2019) Optimal network reconfiguration in active distribution networks with soft open points and distributed generation. Energies 12(21):4172. https://doi.org/10.3390/en12214172

24. Moradi MH, Zeinalzadeh A, Mohammadi Y, Abedini M (2014) An efficient hybrid method for solving the optimal sitting and sizing problem of DG and shunt capacitor banks simultaneously based on imperialist competitive algorithm and genetic algorithm. Int J Electr Power Energy Syst 54:101–111. https://doi.org/10.1016/j.ijepes.2013.06.023
25. Rahmani-Andebili M (2016) Simultaneous placement of DG and capacitor in distribution network. Electr Power Syst Res 131:1–10. https://doi.org/10.1016/j.epsr.2015.09.014
26. Muthukumar K, Jayalalitha S (2016) Optimal placement and sizing of distributed generators and shunt capacitors for power loss minimization in radial distribution networks using hybrid heuristic search optimization technique. Int J Electr Power Energy Syst 78:299–319. https://doi.org/10.1016/j.ijepes.2015.11.019
27. Yazdavar AH, Shaaban MF, El-Saadany EF, Salama MMA, Zeineldin HH (2020) Optimal planning of distributed generators and shunt capacitors in isolated microgrids with nonlinear loads. IEEE Trans Sustain Energy 11(4):2732–2744
28. Elattar EE, Shaheen AM, El-Sayed AM, El-Sehiemy RA, Ginidi AR (2021) Optimal operation of automated distribution networks based-MRFO algorithm. IEEE Access 9:19586–19601
29. Kumar Injeti S, Shareef SM, Kumar TV (2018) Optimal allocation of DGs and capacitor banks in radial distribution systems. Distrib Gener Altern Energy J 33(3):6–34
30. Gampa SR, Das D (2019) Simultaneous optimal allocation and sizing of distributed generations and shunt capacitors in distribution networks using fuzzy GA methodology. J Electr Syst Inf Technol 6(1):1–18
31. Das S, Das D, Patra A (2019) Operation of distribution network with optimal placement and sizing of dispatchable DGs and shunt capacitors. Renew Sust Energ Rev 113:109219. https://doi.org/10.1016/j.rser.2019.06.026
32. Almabsout EA, El-Sehiemy RA, An ONU, Bayat O (2020) A hybrid local search-genetic algorithm for simultaneous placement of DG units and shunt capacitors in radial distribution systems. IEEE Access 8:54465–54481. https://doi.org/10.1109/ACCESS.2020.2981406
33. Shaheen AM, El-Sehiemy RA (2020) Optimal coordinated allocation of distributed generation units/capacitor banks/voltage regulators by EGWA. IEEE Syst J 12:373. https://doi.org/10.1109/JSYST.2015.2491966
34. Safigianni AS, Salis GJ (2000) Optimum voltage regulator placement in a radial power distribution network. IEEE Trans Power Syst 15(2):879–886
35. Dolli SA, Jangamshetti SH (2012) Modeling and optimal placement of voltage regulator for a radial system. In: 2012 international conference on power, signals, controls and computation, pp 1–6
36. Jabbari M, Niknam T, Hosseinpour H (2011) Multi-objective fuzzy adaptive PSO for placement of AVRs considering DGs. In: 2011 IEEE power engineering and automation conference, vol 2, pp 403–406
37. Ranamuka D, Agalgaonkar AP, Muttaqi KM (2016) Examining the interactions between DG units and voltage regulating devices for effective voltage control in distribution systems. IEEE Trans Ind Appl 53(2):1485–1496
38. Ghanegaonkar SP, Pande VN (2015) Coordinated optimal placement of distributed generation and voltage regulator by multi-objective efficient PSO algorithm. In: 2015 IEEE workshop on computational intelligence: theories, applications and future directions (WCI), pp 1–6
39. Rakočević S, Ćalasan M, Abdel Aleem SHE (2021) Smart and coordinated allocation of static VAR compensators, shunt capacitors and distributed generators in power systems toward power loss minimization. Energy Sources, Part A Recover Util Environ Eff:1–19. https://doi.org/10.1080/15567036.2021.1930289
40. International Renewable Energy Agency (2021) Renewable energy Outlook
41. Chakravorty M, Das D (2001) Voltage stability analysis of radial distribution networks. Int J Electr Power Energy Syst 23(2):129–135
42. Dobson I et al (2002) Voltage stability assessment: concepts, practices and tools. IEEE Power Eng Soc Power Syst Stab Subcomm Spec Publ 11:21–22
43. Kersting WH (2018) Distribution system modeling and analysis. CRC Press, Boca Raton

44. Gallego LA, Padilha-Feltrin A (2008) Voltage regulator modeling for the three-phase power flow in distribution networks. In: 2008 IEEE/PES transmission and distribution conference and exposition: Latin America, T and D-LA, pp 1–6. https://doi.org/10.1109/TDC-LA.2008.4641843
45. Kersting WH (2009) The modeling and application of step voltage regulators. In: 2009 IEEE/PES power systems conference and exposition, PSCE 2009, pp 1–8. https://doi.org/10.1109/PSCE.2009.4840004
46. Teng J-H (2003) A direct approach for distribution system load flow solutions. IEEE Trans Power Deliv 18(3):882–887
47. Mirjalili S, Lewis A (2016) The whale optimization algorithm. Adv Eng Softw 95:51–67. https://doi.org/10.1016/j.advengsoft.2016.01.008
48. Ismael SM, Abdel Aleem SHE, Abdelaziz AY (2019) Optimal conductor selection in radial distribution systems using whale optimization algorithm. J Eng Sci Technol 14(1):87–107
49. Elsayed AM, Mishref MM, Farrag SM (2018) Distribution system performance enhancement (Egyptian distribution system real case study). Int Trans Electr Energy Syst 28(6):e2545
50. Diaaeldin I et al (2019) Optimal network reconfiguration in active distribution networks with soft open points and distributed generation. Energies 12(21):4172. https://doi.org/10.3390/en12214172